AD-A134 941 TRANSITION SIMULATION FOR INCOMPRESSIBLE BOUNDARY LAYERS AND HEATED HYDRODYNAMIC BODIES(U) DCW INDUSTRIES SHERMAN OAKS CA D C WILCOX ET AL. JUL 76 DCW-R-10-01 1/1

UNCLASSIFIED N00024-76-C-7070 F/G 20/4 NL

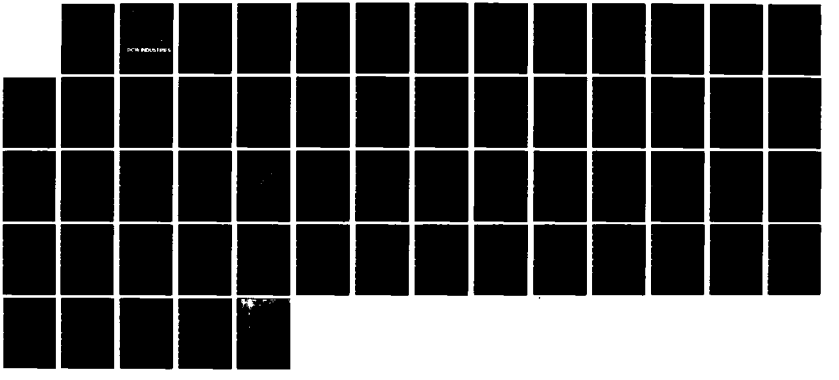

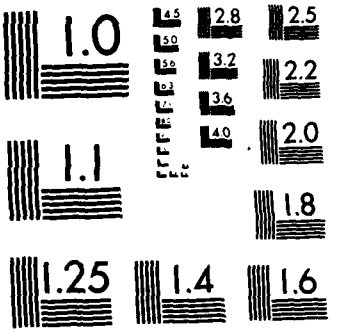

MICROCOPY RESOLUTION TEST CHART
NATIONAL BUREAU OF STANDARDS-1963-A

(1)

78-05-24R

AD-A134 944

TRANSITION SIMULATION FOR INCOMPRESSIBLE BOUNDARY LAYERS AND HEATED HYDRODYNAMIC BODIES

by

D.C. Wilcox and T.L. Chambers

DCW INDUSTRIES

13535 VENTURA BLVD., SUITE 207, SHERMAN OAKS, CALIF. 91423

DCW-R-10-01

TRANSITION SIMULATION FOR INCOMPRESSIBLE BOUNDARY LAYERS AND HEATED HYDRODYNAMIC BODIES

by

D.C. Wilcox and T.L. Chambers

FINAL SCIENTIFIC REPORT

July 1976

Period of Performance: November 1, 1975 to
September 30, 1976

Prepared under Contract N00024-76-C-7070

for the

NAVAL SEA SYSTEMS COMMAND
Alexandria, Virginia

and

DEFENSE ADVANCED RESEARCH PROJECTS AGENCY
Arlington, Virginia

DCW Industries
13535 Ventura Boulevard, Suite 207
Sherman Oaks, California 91423
(213) 990-2682

ABSTRACT

Incompressible boundary-layer transition has been analyzed using a second-order closure turbulence model. With no transition-specific modifications, the turbulence model predicts salient features of incompressible, zero-pressure-gradient boundary-layer transition including sensitivity to freestream turbulence and surface roughness, transition width, and transitional velocity profiles. With transition modifications based on linear stability theory, the model accurately predicts transition sensitivity to surface heat transfer, pressure gradient, and suction. With no further modifications, transition predictions have been made for several hydrodynamic bodies, including effects of surface heating.

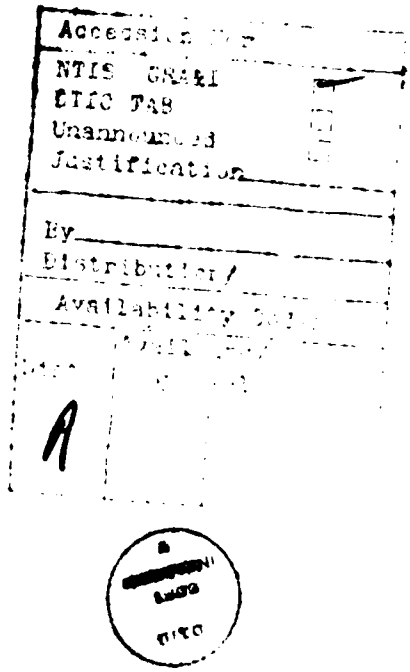

ACKNOWLEDGEMENT

The authors gratefully express their appreciation to Carl Gazley of The RAND Corporation for providing timely information needed during the course of this study. Also, Joel Granet of NAVSEA provided important guidance in expediting performance of contract tasks.

CONTENTS

LIST OF ILLUSTRATIONS

LIST OF ILLUSTRATIONS (concluded)

NOTATION

SYMBOL	DEFINITION
c_f	Local skin friction
C_p	Pressure coefficient, $(p-p_\infty)/\frac{1}{2}\rho U_\infty^2$
C_Q	Volume coefficient, $-\rho_w v_w/\rho_e U_e$
e	Specific turbulent mixing energy [Equation (12)]
e_{max}	Maximum value of e in boundary layer
$f(\Lambda), F\{\Lambda; T'_{max}\}$	Stability functions [Equations (34)]
h	Mean specific enthalpy
$H(\Lambda)$	Heaviside stepfunction
k	Roughness height (peak-to-valley)
L	Body length measured along symmetry axis
N_e, N_ω	Roughness functions [Equations (22,23)]
p	Static pressure
Pr_L, Pr_T	Laminar, turbulent Prandtl number
q	Local heat flux [Equation (8)]
r	Radial distance from body axis
Re_c	Minimum critical Reynolds number
$Re_{\hat{x}}$	Neutral stability Reynolds number
$Re_{k,x,s,\delta^*,V^{1/3}}$	Reynolds number based on roughness height, plate length, arclength, displacement thickness, cube root of volume
Re_T	Turbulent Reynolds number [Equation (11)]
s	Arclength
s_{min}, s_{max}	Arclengths between which Body 2 is heated
s_{mr}	Arclength at which body radius is a maximum
S, S_B, S_R	Roughness functions [Equations (19,20,21)]

NOTATION (continued)

SYMBOL	DEFINITION
T	Mean temperature
T'	Turbulence intensity at boundary-layer edge
T'_{max}	Maximum value of T' in boundary layer
u,v	Mean velocity components in s,y directions
u_τ	Friction velocity, $\sqrt{\tau_w/\rho_w}$
v'	Fluctuating velocity in y direction
V	Body volume
x	Plate length
α,α^*	Parameters in model equations
$\alpha_\infty,\alpha^*_\infty$	Values of α,α^* for fully turbulent flows
$\tilde{\alpha}$	Wave number
β,β^*	Parameters in model equations
δ	Boundary layer thickness
δ^*	Displacement thickness
ε	Kinematic eddy viscosity
θ	Momentum thickness
λ	Parameter in model equations
Λ	Stability parameter [Equations (28)]
μ	Molecular viscosity
ν	Kinematic molecular viscosity
ρ	Mean density
σ,σ^*	Parameters in model equations
τ	Shear stress [Equation (7)]
ω	Turbulent dissipation rate [Equation (13)]
ℓ	Turbulent length scale [Equation (9)]

NOTATION (concluded)

SUBSCRIPTS	DEFINITION
e	Boundary-layer edge
t	Transition point
w	Body surface
∞	Freestream

1. INTRODUCTION

Current design techniques for low-drag hydrodynamic bodies require accurate prediction of transition from laminar to turbulent flow. For example, guided by linear stability predictions, judicious use of various factors such as surface heating and pressure gradient has delayed transition to arclength Reynolds numbers in excess of 40 million for small hydrodynamic bodies. Based on this success, larger laminar-flow vehicles have been proposed for which transition Reynolds numbers must be in excess of 200 million. Again design procedures depend mainly upon linear stability theory.

Because of the expense involved in building these larger vehicles, transition sensitivity to several additional factors must be established to insure feasibility of the design. Potentially detrimental effects of surface roughness, freestream turbulence, vibration and acoustic disturbances must be established. Because of the paucity of experimental data pertaining to such factors, the designer must turn to theoretically-based predictive methods. While linear stability theory is adequate for predicting effects of primary design parameters such as pressure gradient and surface heating, stability theory has no natural way of simulating effects of surface roughness and freestream disturbances. Alternate methods which simulate transition sensitivity to roughness and freestream disturbances thus have potential utility in the design of large laminar-flow vehicles.

One such method is based on second-order closure turbulence models. As shown by Wilcox and Chambers,[1-6] transition sensitivity to many of the effects pertinent to hydrodynamic boundary layers can be predicted with reasonable accuracy using turbulence model equations. While this method displays great potential for engineering design, confidence in the basic formulation requires further bolstering. Two key points require clarification. Most significant, an explanation is needed for the manner in which Tollmien-Schlichting

waves manifest themselves in the theory. The second point is that model predictions display a strong sensitivity to freestream disturbances which has been substantiated by limited experimental measurements; further substantiation is needed.

The purpose of this study has been twofold. First, an explanation has been sought for the way in which the turbulence-model approach accommodates Tollmien-Schlichting waves. Second, turbulence-model transition predictive accuracy has been assessed for the various effects pertinent to transition on hydrodynamic vehicles, including freestream disturbances. Section 2 presents the model equations upon which the study is based. Appropriate transition modifications to the fully turbulent form of the equations are devised, and the model's relation to stability theory is delineated. Section 3 summarizes results of classical incompressible boundary-layer applications including comparison of predicted and measured effects on boundary-layer transition of freestream turbulence, surface roughness, pressure gradient, suction and surface heat transfer. In Section 4, the model is used to predict transition on four hydrodynamic bodies with and without surface heating. The concluding section summarizes results and conclusions.

2. EQUATIONS OF MOTION

The turbulence/transition model equations are summarized in this section including established values of all closure coefficients. Subsection 2.1 presents the model equations including physical meanings of turbulence field properties. Subsection 2.2 specifies surface boundary conditions for flow over rough surfaces with mass transfer. Subsection 2.3 gives details of special modifications needed to obtain accurate predictions for effects on transition of pressure gradient and surface heat transfer. In Subsection 2.4, the manner in which Tollmien-Schlichting waves manifest themselves in the theory is explained.

2.1 THE TURBULENCE/TRANSITION MODEL

Under the standard boundary-layer approximations, the model equations for two-dimensional (j=0) and axisymmetric (j=1) incompressible flows are

Mass Conservation

$$\frac{\partial u}{\partial s} + \frac{1}{r^j}\frac{\partial}{\partial y}(r^j v) = 0 \tag{1}$$

Momentum Conservation

$$\rho u\frac{\partial u}{\partial s} + \rho v\frac{\partial u}{\partial y} = -\frac{dp}{ds} + \frac{\partial \tau}{\partial y} \tag{2}$$

Energy Conservation

$$\rho u\frac{\partial h}{\partial s} + \rho v\frac{\partial h}{\partial y} = u\frac{dp}{ds} - \frac{\partial q}{\partial y} \tag{3}$$

Turbulent Mixing Energy

$$\rho u\frac{\partial e}{\partial s} + \rho v\frac{\partial e}{\partial y} = \left[\alpha^*\left|\frac{\partial u}{\partial y}\right| - \beta^*\omega\right]\rho e + \frac{\partial}{\partial y}\left[(\mu+\sigma^*\rho\varepsilon)\frac{\partial e}{\partial y}\right] \tag{4}$$

Turbulent Dissipation Rate

$$\rho u\frac{\partial \omega^2}{\partial s} + \rho v\frac{\partial \omega^2}{\partial y} = \left\{\alpha\left|\frac{\partial u}{\partial y}\right| - \left[\beta + 2\sigma\left(\frac{\partial \ell}{\partial y}\right)^2\right]\omega\right\}\rho\omega^2 + \frac{\partial}{\partial y}\left[(\mu+\sigma\rho\varepsilon)\frac{\partial \omega^2}{\partial y}\right] \tag{5}$$

where s and y are orthogonal coordinates with s lying along the body (arclength) and y being normal to the surface; r is the radial distance from the body axis. Mean velocity components in the s and y directions are denoted by u and v while h is the specific enthalpy; p, ρ and μ are mean density, pressure, and molecular viscosity; τ and q are the shear stress and normal heat flux. The turbulent mixing energy, e, and the turbulent dissipation rate, ω, are needed to define the eddy diffusivity, ε, which is given by the following equation:

$$\varepsilon = e/\omega \tag{6}$$

The shear stress and heat flux are

$$\tau = (\mu+\rho\varepsilon)\frac{\partial u}{\partial y} \tag{7}$$

$$q = -\left(\frac{\mu}{Pr_L} + \frac{\rho\varepsilon}{Pr_T}\right)\frac{\partial h}{\partial y} \tag{8}$$

where Pr_L and Pr_T are laminar and turbulent Prandtl numbers. The quantity ℓ is the turbulent length scale defined as

$$\ell = e^{1/2}/\omega \tag{9}$$

The turbulent Prandtl number, Pr_T, and the closure coefficients $\alpha,\alpha^*,\beta,\beta^*,\sigma,\sigma^*$ appearing in Equations (4) and (5) are

$$\left.\begin{aligned} \beta &= \frac{3}{20} & \beta^* &= \frac{9}{100} \\ \sigma &= \frac{1}{2} & \sigma^* &= \frac{1}{2} \\ & Pr_T = \frac{8}{9} & & \\ \alpha &= \frac{1}{3}\left[1 - (1-\lambda)\exp(-Re_T/2)\right] & & \\ \alpha^* &= \frac{3}{10}\left[1 - (1-\lambda)\exp(-2Re_T)\right] & & \end{aligned}\right\} \tag{10}$$

where Re_T is the turbulent Reynolds number defined by

$$Re_T = \rho e^{\frac{1}{2}} \ell / \mu \tag{11}$$

Specification of the closure coefficient λ is deferred to Subsection 2.3.

Consistent with the arguments of Wilcox and Chambers,[2,4] the turbulent mixing energy is proportional to the kinetic energy attending the fluctuation of fluid particles normal to the plane of shear. Letting v' denote the fluctuating velocity component normal to the shear plane (under the boundary-layer approximations, shear planes are parallel to the s direction), the turbulent mixing energy is given by

$$e = \frac{9}{4} \langle v'^2 \rangle \tag{12}$$

where $\langle\ \rangle$ denotes time average.

The physical meaning of ω has been discussed by Wilcox.[2] For incompressible boundary layers, comparison of the limiting forms of the model equations and the exact Reynolds stress equation very close to a solid boundary shows that ω is the rate at which e is dissipated into heat, mean kinetic energy and other fluctuation modes. For incompressible flows, Wilcox deduced that

$$\omega = \frac{3\nu}{\beta^*} \frac{\langle (\partial v'/\partial y)^2 \rangle}{\langle v'v' \rangle} \tag{13}$$

where $\nu = \mu/\rho$ is kinematic viscosity.

2.2 BOUNDARY CONDITIONS

Boundary conditions for the model must be specified at a solid boundary (y=0) and at the boundary-layer edge ($y=\delta$). Suitable boundary conditions have been devised by Wilcox and Chambers;[4,5] for completeness, the boundary conditions are summarized in this subsection.

For mean flow properties, conditions are the same as for a standard boundary-layer computation. The velocity satisfies the no-slip condition at y=0 while either the surface temperature, T_w, or the surface heat flux, q_w, is specified. Hence

$$\left.\begin{aligned} u &= 0 \quad , \quad v = v_w \\ T &= T_w \quad \text{or} \quad \partial T/\partial y = -\,Pr_L\, q_w/\mu_w \end{aligned}\right\} \quad \text{at} \quad y = 0 \qquad (14)$$

At the boundary-layer edge, velocity and temperature assume prescribed values; we thus write

$$\left.\begin{aligned} u &= U_e \\ T &= T_e \end{aligned}\right\} \quad \text{at} \quad y = \delta \qquad (15)$$

Turning now to the turbulence parameters e and ω, edge boundary conditions are most conveniently expressed in terms of the free-stream turbulence intensity, T', and the turbulent length scale, $\ell = e^{1/2}/\omega$. For transition applications, we generally use (see Subsection 3.1)

$$\left.\begin{aligned} e_e &= \tfrac{3}{2}(T'/100)^2\, U_e^2 \\ \ell_e &= .004\, \sqrt{\alpha_\infty^*}\,\delta \end{aligned}\right\} \quad \text{at} \quad y = \delta$$

where $\alpha_\infty^* = 3/10$ is the high Reynolds number ($Re_T >> 1$) limiting value of α^* and T' is given in per cent, i.e.,

$$T' \equiv 100\sqrt{\tfrac{1}{3}\langle u_e'^2 + v_e'^2 + w_e'^2\rangle}/U_e \qquad (17)$$

Finally, the surface boundary conditions for e and ω are

$$\left.\begin{aligned} e &= \frac{N_e}{\alpha_\infty^*}\,\frac{\nu_w^2}{k^2} \\ \omega &= \frac{S}{\alpha_\infty^*}\,\frac{u_\tau^2}{\nu_w} \end{aligned}\right\} \qquad (18)$$

where k is roughness height, u_τ is friction velocity, and $c_f = \sqrt{u_\tau/U_e}$ is skin friction. The quantity S is a univesal function of surface

roughness and mass injection which has been determined by extensive study of viscous sublayer properties; S is given by

$$S = \left[\frac{1}{S_B} + \frac{1}{S_R N_\omega}\right]^{-1} \tag{19}$$

where

$$S_R = \left(\frac{36}{u_\tau k/\nu_w}\right)^2 + \left(\frac{8}{u_\tau k/\nu_w}\right)^{1/2} \tag{20}$$

and

$$S_B = \begin{cases} 6\dfrac{(\nu_w/u_\tau)^{-1}}{1+(\nu_w/u_\tau)} & ; \quad \nu_w/u_\tau > 0 \\ 0 & ; \quad \nu_w/u_\tau \leq 0 \end{cases} \tag{21}$$

In analyzing the viscous sublayer, the two functions N_e and N_ω were taken to be unity. For transition applications, N_e and N_ω vary with the dimensionless grouping $c_f/(k/\theta)$. Such a dependence has been introduced to facilitate use of a boundary-layer computation for predicting transition; having $N_e = N_\omega = 1$ would require an elliptic integration method to account for local flow separation between roughness elements (see Wilcox and Chambers[4,5] for further details). The functions N_e and N_ω have been found by numerical experimentation; their postulated dependence upon $c_f/(k/\theta)$ is

$$N_e = \begin{cases} 0 & , \quad u_\tau k/\nu_w < 5 \\ .001\left[\dfrac{275\ c_f}{k/\theta}\right]^{-4} & , \quad u_\tau k/\nu_w \geq 5 \end{cases} \tag{22}$$

$$N_\omega = \begin{cases} 1 & , \quad k/\theta \leq 275\ c_f \\ \left[\dfrac{275\ c_f}{k/\theta}\right]^6 & , \quad k/\theta > 275\ c_f \end{cases} \tag{23}$$

2.3 TRANSITION MODIFICATIONS

Of the various closure coefficients, model-predicted transition is most sensitive to the coefficient λ appearing in Equations (10). As argued by Wilcox,[1] the value of λ can be determined by demanding that the model equations predict that in a Blasius boundary layer turbulent fluctuations are damped for Reynolds numbers below the linear-stability-theory minimum-critical Reynolds number, Re_c. Having mixing-energy production, $\alpha^*|\partial u/\partial y|e$, less than mixing energy dissipation, $\beta^*\omega e$, insures such damping. Using the Blasius velocity profile and the smooth wall ω profile (i.e., $\omega = 20\nu/\beta y^2$ – see Appendix), the maximum plate-length Reynolds number, $Re_{\hat{x}}$, at which dissipation is greater than or equal to production throughout the boundary layer is

$$Re_{\hat{x}} \doteq 750/\lambda^2 \tag{24}$$

The Reynolds number $Re_{\hat{x}}$ will be equal to $9 \cdot 10^4$, the accepted value of Re_c, provided

$$\lambda \doteq 1/11 \tag{25}$$

With λ given by Equation (25), Wilcox and Chambers[5] (see Subsection 3.1) have shown that the model accurately simulates many aspects of transition for an incompressible flat-plate boundary layer (FPBL) including transition sensitivity to freestream turbulence, transition width, and transitional velocity profiles. However, previous experience[3] with heated hydrodynamic boundary layers shows that in order to accurately predict effects of pressure gradient and surface heat transfer, Equation (25) must be modified. The remainder of this subsection is devoted to explaining the need for and specification of further modifications to the closure coefficient λ.

As noted above, the value of λ has been fixed by demanding that the linear-stability minimum-critical Reynolds number, Re_c, for the Blasius boundary layer match the corresponding model-equation

neutral-stability Reynolds number, $Re_{\hat{x}}$. Demanding that $Re_c = Re_{\hat{x}}$ for the Blasius boundary layer yields the value of λ given in Equation (25). The model equations reasonably can be expected to apply to transitional flows which are insensitive to spectral effects. That is, the various constants in the model equations are essentially correlation coefficients which have been integrated over the turbulent spectrum. Hence, if the stability diagram shows that a wide range of wave numbers, $\tilde{\alpha}$, undergo amplification, the spectrum will more closely resemble a fully-turbulent spectrum than if only a small range of wave numbers are unstable. For example, the stability diagram for a boundary layer subjected to a pressure gradient is shown in Figure 1. For adverse pressure gradient, a finite range of wave numbers are unstable at all Reynolds numbers in excess of Re_{x_c} (note that δ^* is displacement thickness). On the basis of the discussion above, the model would be expected to accurately predict the destabilizing effect of adverse pressure gradient. In contrast, the stability diagram becomes thinner with increasing favorable pressure gradient so that spectral effects become increasingly important, particularly for small T' which yields transition at large values of Re_{δ^*}; the model hence would be expected to fare poorly for transitional boundary layers with favorable gradients (and small freestream disturbances).

As shown by Wilcox and Chambers,[4] the original version of the model behaves just as the above discussion indicates. Excellent agreement between theory and experiment is obtained for adverse gradients while, for low freestream turbulence intensities, the model fails to predict the strong stabilizing effect of favorable gradient. To remove this deficiency, Wilcox and Chambers[4] introduced an empirical modification to Equation (25). While reasonably good agreement with measurements resulted, the modification lacked rigor.

In the present study, a better approach to modifying λ has been found. That is, the requirement

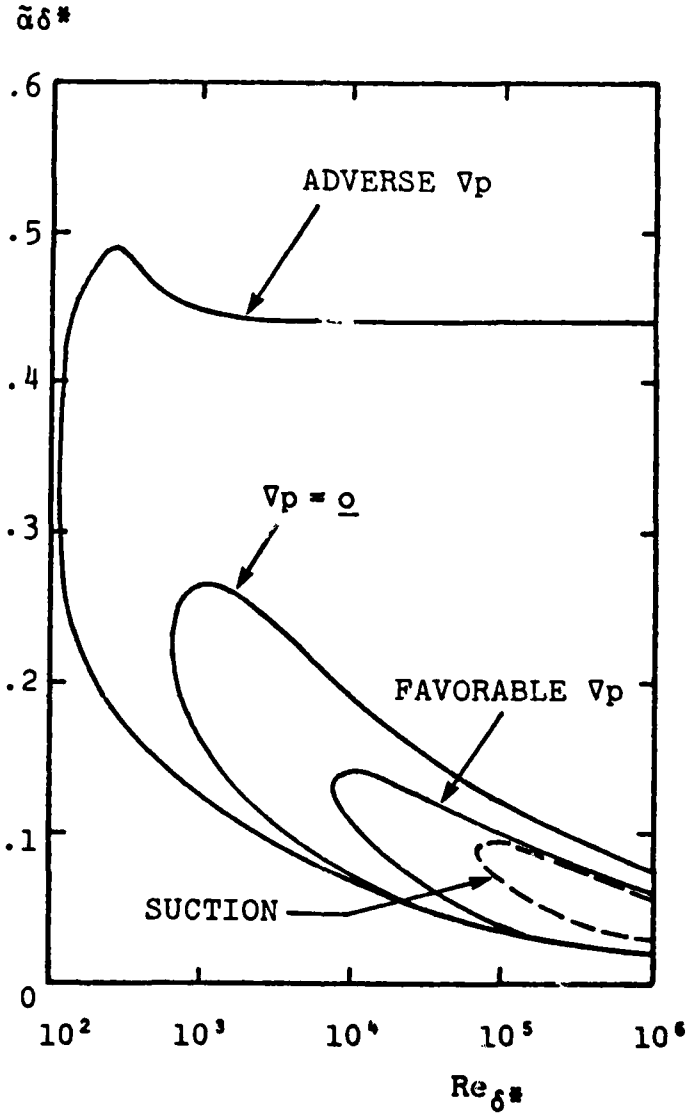

Figure 1. Neutral stability curves for laminar boundary layers with pressure gradient and suction.

$$Re_c = Re_{\hat{x}} \tag{26}$$

has been extended to include favorable pressure gradients. Hence, for small freestream turbulence intensity we expect to have

$$\lambda = \frac{1}{11} f(\Lambda) \quad \text{as} \quad T' \to 0 \tag{27}$$

where Λ is the modified Pohlhausen pressure gradient parameter

$$\Lambda = \frac{\rho_e}{\rho_w} \frac{\theta^2}{\nu_e} \frac{dU_e}{ds} = -\frac{\rho_e}{\rho_w} \frac{\theta^2}{U_e} \left(\frac{\partial^2 u}{\partial y^2}\right)_w \tag{28}$$

The function $f(\Lambda)$ must be determined by equating Re_c and $Re_{\hat{x}}$. Figure 2 presents results based on the Phlhausen profiles[7]; a good fit to the data indicate the variation of λ with Λ is hence

$$f(\Lambda) \doteq \frac{1}{88} + \frac{87}{88} \exp\left[-40\Lambda H(\Lambda)\right] \tag{29}$$

where $H(\Lambda)$ is the Heaviside stepfunction. The limiting value of $f(\Lambda)$ as $\Lambda \to 0$ has been obtained by a similar analysis of the asymptotic laminar profile for a uniformly-sucked FPBL.

Turning to heat transfer, an additional modification to λ is needed. Following Wilcox and Chambers,[3] for incompressible aerodynamic boundary layers with heat transfer, the neutral stability Reynolds number based on wall conditions is given by

$$Re_{\hat{x}_w} \equiv \frac{U_e \hat{x}}{\nu_w} \doteq \frac{750}{\lambda^2} \tag{30}$$

According to linear stability theory,[8] the corresponding minimum-critical Reynolds number Re_{c_w} varies as follows:

$$Re_{c_w} \sim (T_w/T_e)^{-7} \tag{31}$$

Hence, since $\mu \sim T^{0.7}$ for air, we have

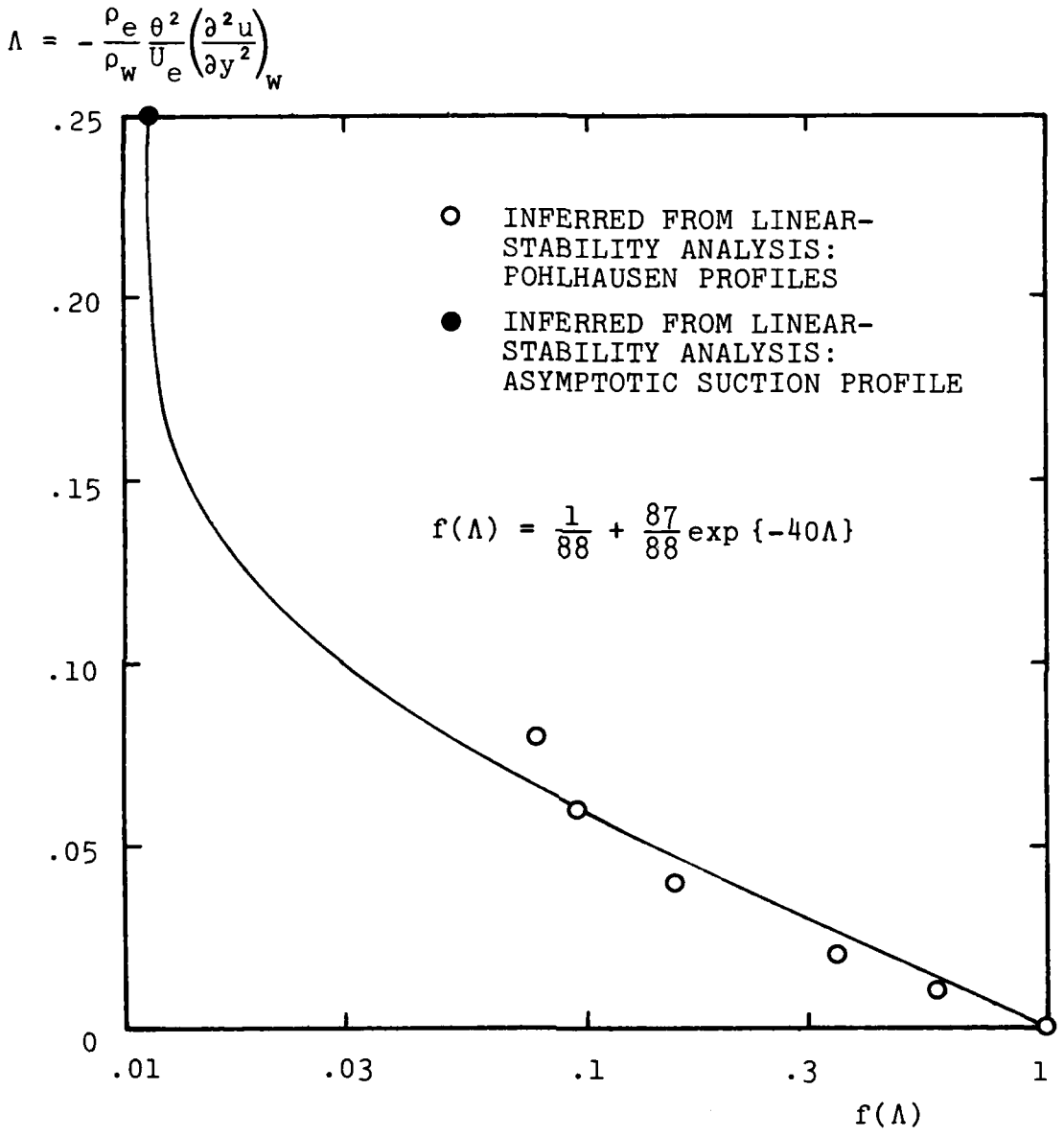

Figure 2. The stability function f(Λ).

$$Re_{c_w} \sim (\mu_w/\mu_e)^{-5} \tag{32}$$

We thus postulate that for flows with heat transfer, λ be written as follows:

$$\lambda = \frac{1}{11}\left(\frac{\mu_w}{\mu_e}\right)^{5/2} F\{\Lambda\ ;\ T'_{max}\} \tag{33}$$

Finally, note that for high freestream turbulence intensities, transition is unlikely to be sensitive to spectral effects regardless of the stability diagram. That is, typical high intensity freestream turbulence will have fluctuations at all frequencies (wave numbers). Therefore, the modification proposed in Equation (33) is strictly valid only as $T' \to 0$. Hence, to complete the formulation, we introduce an exponential dependence upon T'_{max}, the maximum disturbance in the boundary layer, so that the completed formulation is as follows.

TRANSITION MODIFICATION

$$\lambda = \frac{1}{11}\left(\frac{\mu_w}{\mu_e}\right)^{5/2} F\{\Lambda\ ;\ T'_{max}\}$$

$$F\{\Lambda\ ;\ T'_{max}\} = 1 + [f(\Lambda)-1]\exp[-3T'^{2}_{max}]$$

$$f(\Lambda) = \frac{1}{88} + \frac{87}{88}\exp[-40\Lambda H(\Lambda)] \tag{34}$$

where

$$\Lambda = -\frac{\rho_e}{\rho_w}\frac{\theta^2}{U_e}\left(\frac{\partial^2 u}{\partial y^2}\right)_w \quad \text{and} \quad T'_{max} = 100\sqrt{\frac{2}{3}e_{max}}/U_e$$

2.4 WHAT HAPPENED TO THE TOLLMIEN-SCHLICHTING WAVES?

Before proceeding to applications, it is instructive to discuss the key aspect of the turbulence-model transition-prediction method requiring clarification, namely, the manner in which Tollmien-Schlichting waves manifest themselves in the theory. Because we are solving the conventional long-time (Reynolds) averaged equations of motion, no wave-like motion can be discerned. Hence, the whole stability mechanism can only be represented implicitly with the model equations. The arguments presented in Subsection 2.3, particularly the point that the various closure coefficients are correlation coefficients which have been integrated over the wave-number spectrum, illustrate the manner in which Tollmien-Schlichting wave-stability information is implied. Clearly the wave-number spectrum of a given correlation coefficient associated with initiation and early amplification of Tollmien-Schlichting waves is likely to be quite different from the corresponding spectrum in fully turbulent flow. Thus, the values of the closure coefficients α and α^* at the beginning of transition differ markedly from the values appropriate for fully turbulent flows.

Analysis of the viscous sublayer indicates that α and α^* are smaller at low Reynolds numbers than at higher Reynolds numbers, the ratio being λ, i.e.,

$$\frac{\alpha^*(Re_T = 0)}{\alpha^*(Re_T \to \infty)} = \lambda \tag{35}$$

and similarly for α. While the value quoted in Equation (25) is sufficient to yield accurate sublayer structure and transition predictions for the FPBL, we have found that a constant value for λ is insufficient to provide an accurate model for more general transition applications. It is through the precise value of λ that the Tollmien-Schlichting waves implicitly appear in the model. Because the only transition-specific modifications to the

model equations are for the coefficient λ, it is hence unsurprising that ultimately we have chosen to rely upon linear stability theory to set its value.

Given this insight, the whole concept of using turbulence-model equations to describe transition can be cast in a different light. On the one hand, time-averaging conceals many important physical aspects of transition mechanisms, particularly during the early linear-amplification phase. We are thus obligated to put some of the physics back into the equations which was lost through the time-averaging process; ergo, the modification to λ. On the other hand, assuming the latter phases of transition to be very rapid, the time-averaging process becomes a more plausible concept as the flow more nearly resembles a turbulent flow. Interestingly, the modification to λ has little effect on the latter stages of transition. The turbulence-model transition-prediction approach thus has its strongest foundation in the latter stages of transition, precisely the regime where conventional linear-stability methods are not well founded.

To explain this last point, note that the classical Smith-Gamberoni[9] e^9 method ignores nonlinear effects in a region where such effects certainly have a strong effect on the transition process. Thus, turbulence-model equations might most properly be viewed as a plausible alternative to the e^9 method. That is, a linear stability computation could be performed up to, and perhaps a bit beyond, the minimum critical Reynolds number. Results of the stability computation would define λ. Then rather, than continuing to solve eigenvalue problems to determine amplification factors up to the e^9 amplification point, the model equations could be used to predict transition location. What we are currently doing is using a correlation of linear stability minimum critical Reynolds numbers to fix the value of λ.

All of the comments above pertain to transition triggered by disturbances of sufficiently low amplitude for linear stability theory to be relevant. However, if large amplitude freestream or roughness-induced disturbances are present, the bypass phenomenon[10] may occur, in which case Tollmien-Schlichting waves are irrelevant. Because the turbulence/transition model accurately simulates bypass,[4] most notably for roughness-induced transition, the current formulation enjoys an interesting advantage over linear-stability methods for flows with large amplitude disturbances.

3. BOUNDARY LAYER APPLICATIONS

To test the model, we first consider carefully-documented experiments for conventional incompressible boundary layers. This section presents results of five applications, all of which are pertinent to low-drag hydrodynamic vehicles. First, we apply the model to an incompressible FPBL including comparisons of computed and measured transitional velocity profiles, transition width and transition sensitivity to freestream turbulence intensity and scale. Then, we simulate the effects of surface roughness, pressure gradient and suction. In the concluding subsection, we use the model to analyze effects of surface heat transfer on aerodynamic boundary layers.

3.1 FREESTREAM TURBULENCE[†]

As the first step in testing the model, we analyze various aspects of model-predicted incompressible FPBL transition. As shown in Figure 3, starting from laminar flow at the plate leading edge, the model predicts that the skin friction initially matches the Blasius value. Then, depending upon the freestream turbulence intensity, T', skin friction rapidly increases at a critical Reynolds number, Re_{x_t}, and asymptotically approaches the equilibrium turbulent value. Predicted variation of c_f closely resembles that observed when a boundary layer undergoes transition to turbulence.

For example, Figure 4 shows that, consistent with measurements,[11] momentum-thickness Reynolds number at transition, Re_{θ_t}, varies almost linearly with T' for low-intensity freestream turbulence (i.e., T' less than 1%). (The criterion used to define transition

[†] Some of the results presented in this subsection were obtained in Contract F44620-74-C-0048.

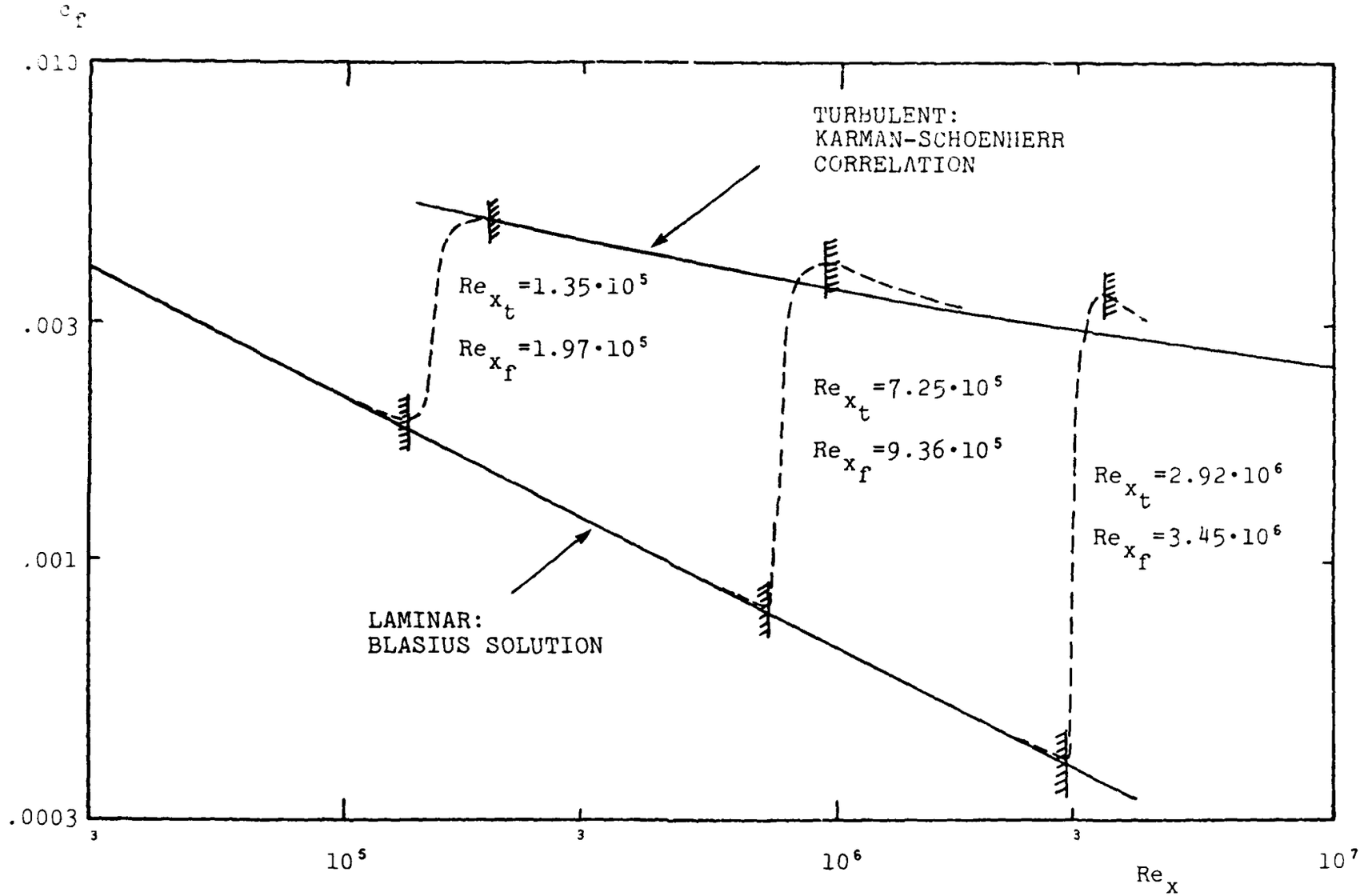

Figure 3. Computed variation of skin friction with Re_x for transitional boundary layers; transition region lies between points at which minimum and maximum c_f occur.

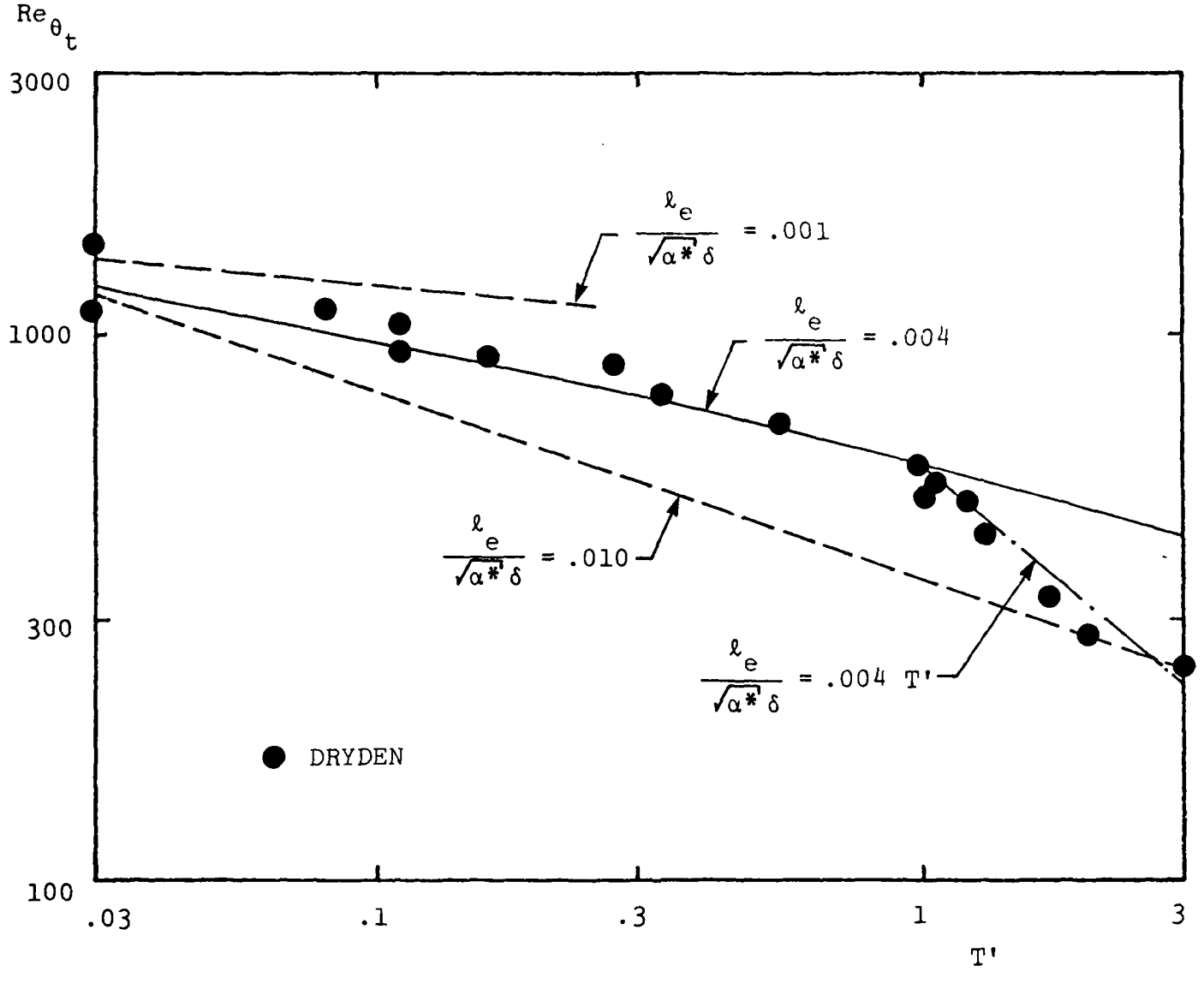

Figure 4. Effect of freestream turbulence intensity on transition location for a flat-plate boundary layer.

is the point at which c_f achieves a minimum.) Note that turbulence scale has an effect on Re_{θ_t}, particularly for T' > 1%. Computations have been performed with various ratios of $\ell_e/\sqrt{\alpha^*_\infty}$ to δ; having $\ell_e/\sqrt{\alpha^*_\infty}\delta$ given by

$$\frac{\ell_e}{\sqrt{\alpha^*_\infty}\,\delta} = .004 \; ; \; T' < 1 \tag{36}$$

most nearly matches the low-intensity values of Re_{θ_t}. Somewhat larger values of $\ell_e/\sqrt{\alpha^*_\infty}\delta$ are needed to match the high-intensity data; for values of T' in excess of 1%, excellent agreement between computed and measured Re_{θ_t} is obtained with $\ell_e/\sqrt{\alpha^*_\infty}\delta$ given by

$$\frac{\ell_e}{\sqrt{\alpha^*_\infty}\,\delta} = .004T' \; ; \; T' > 1 \tag{37}$$

Intuitively, we expect that ℓ_e should increase with T' for high-intensity turbulence since, in the case of fully turbulent boundary layers, values of $\ell_e/\sqrt{\alpha^*_\infty}\delta$ generally are an order-of-magnitude greater than that given by Equation (36). The variation of ℓ_e with T' given by Equation (37) is quite plausible since the peak local intensity in a fully turbulent incompressible FPBL is of the order of 10 to 12% which, from Equation (37) indicates $\ell_e/\sqrt{\alpha^*_\infty}\delta$ is of the order .04 to .05. For turbulent boundary layers, $\ell_e/\sqrt{\alpha^*_\infty}\delta$ is typically .09.

In Figure 5, predicted width of the transition region is compared with measured[12] width. Transition width, Δx_t, is defined as the distance between minimum and maximum skin-friction points. Using this definition for Δx_t, Reynolds number based on Δx_t was computed for Re_{x_t} ranging from $5.0 \cdot 10^4$ to $4.4 \cdot 10^6$. As shown, the computed curve falls within experimental data scatter.

Figure 6 exhibits computed and measured[13] velocity profiles through transition for T' = .03%. Comparison of velocity profiles at x = 5.75 ft indicates the computed boundary layer goes turbulent a bit faster than measured. Proceeding downstream, however, computed

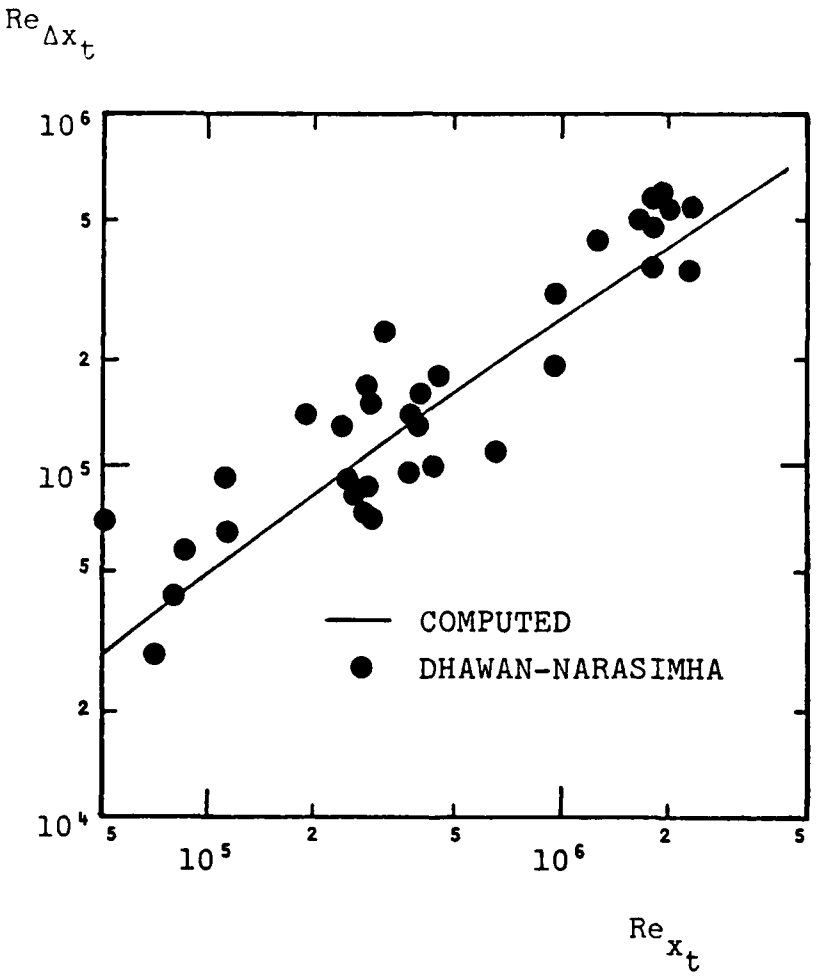

Figure 5. Comparison of computed and measured Reynolds number based on transition-zone width.

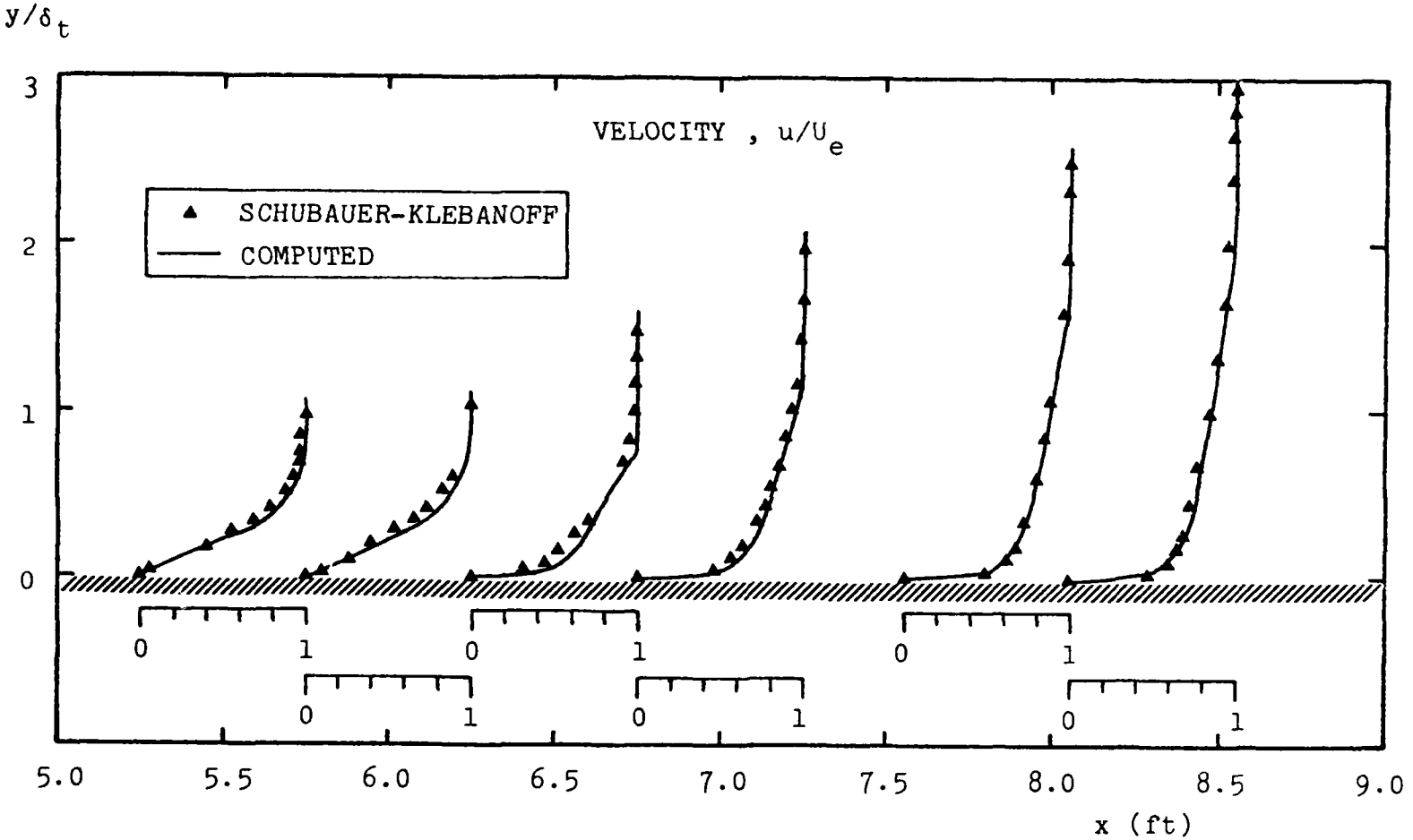

Figure 6. Comparison of computed and measured transitional velocity profiles for an incompressible flat-plate boundary layer; $T' = .03\%$; $\ell_e/\sqrt{\alpha^*_\infty} = .09$; $Re_\infty = 5.2 \cdot 10^5$ per foot.

and measured velocity profiles show decreasing differences until, beyond $x = 6.75$ ft, differences are less than 5%.

An interesting point about these results is that because $(\partial^2 u/\partial y^2)_w$ vanishes for incompressible FPBL flow, the transition modification defined in Equation (34) has no effect. Hence, the turbulence model as stated in Subsection 2.1 applies, with $\lambda = 1/11$, to the incompressible FPBL.

3.2 SURFACE ROUGHNESS

Figure 7 shows computed effects of surface roughness on FPBL transition; experimental data of Feindt[14] are shown for comparison. Freestream intensity has only a slight effect on transition Reynolds number based on plate length, Re_{x_t}, for roughness-height Reynolds numbers in excess of 300. Thus, consistent with qualitative observations, the model predicts existence of a roughness dominated regime, although substantiating data are unavailable for determining the minimum value of Re_k at which transition becomes roughness dominated. Also, again consistent with measurements and qualitative observations, roughness has virtually no effect on FPBL transition for $Re_k \lesssim 120$.

3.3 PRESSURE GRADIENT

Figure 8 compares predicted and measured effects of pressure gradient on FPBL transition. As shown in the figure, the Crabtree[15] data are closely simulated by the computations with $T' = .01\%$ and $.03\%$. Since the Crabtree data are for flight tests (closed circles) and quiet wind tunnels (open circles), the value of T' for the experiments would be expected to fall in the range .01%-.03%. The agreement between theory and experiment hence is very good for low intensities. Additionally, the Feindt[14] high-intensity data ($T' = 1.25\%$) are closely matched by the computed curve with $T' = 1.25\%$; because Feindt found that transition occurs ahead of the minimum critical Reynolds number for favorable gradient, this flow exhibits an example of the bypass phenomenon.

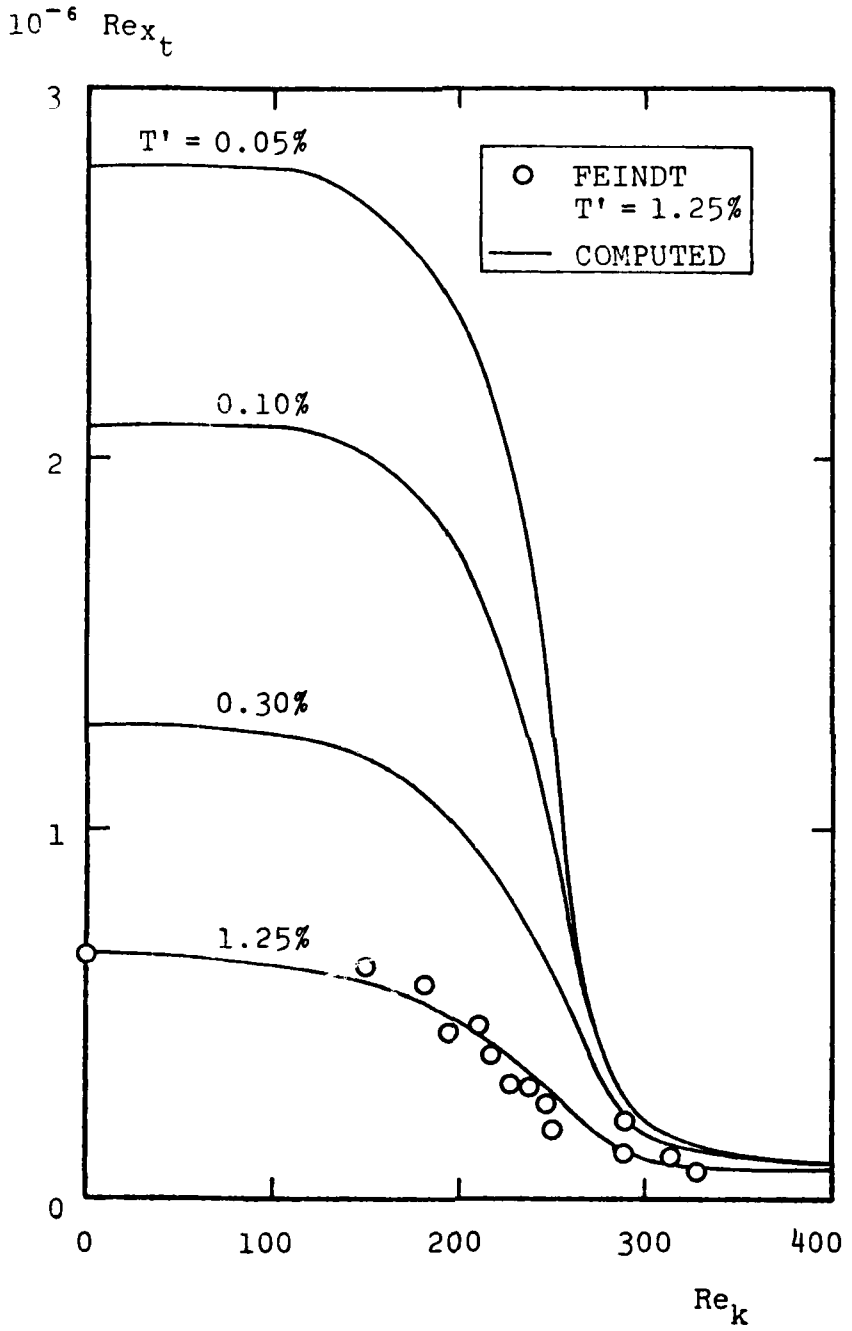

Figure 7. Effect of surface roughness on flat-plate boundary-layer transition.

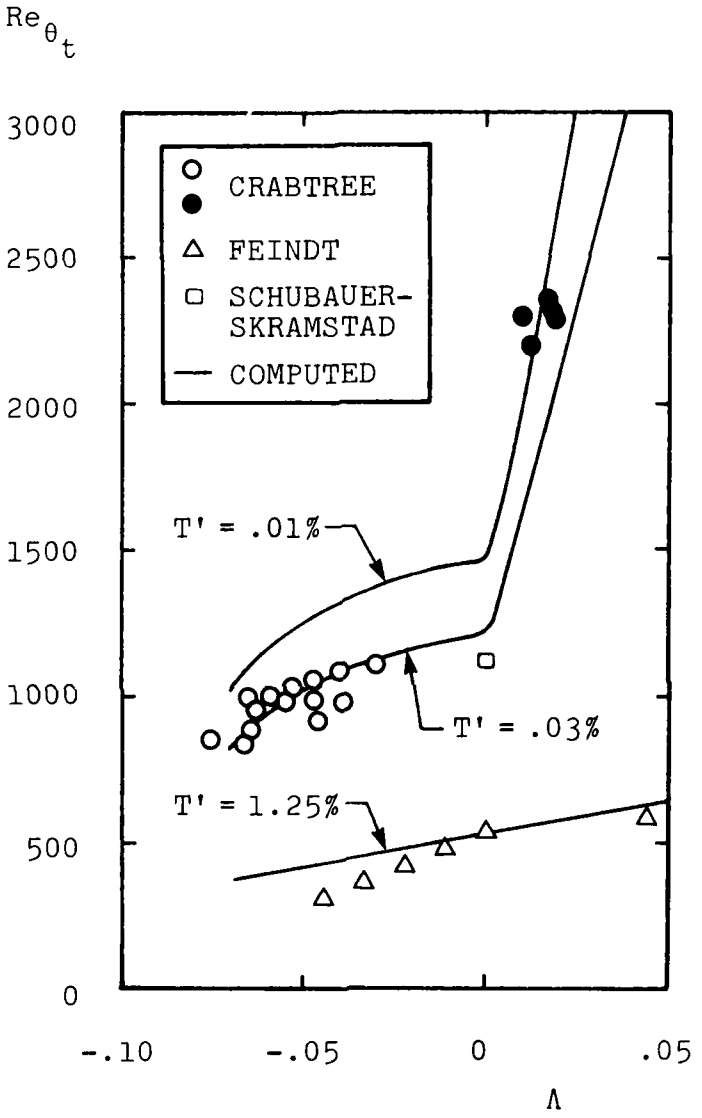

Figure 8. Comparison of computed and measured effects of pressure gradient on boundary-layer transition.

3.4 SUCTION

Figure 9 shows computed minimum volume coefficient, $C_{Q_{min}}$, required to prevent transition of a FPBL with uniform suction. Volume coefficient is defined as

$$C_Q \equiv -\frac{\rho_w v_w}{\rho_e U_e} \tag{38}$$

where v_w is suction velocity. As shown, for values of T' above about 0.3%, $C_{Q_{min}}$ is .0012, a value typical[16,17] of experiments performed in noisy wind tunnels. As expected, our numerical computations confirm that in the limit $T' \to 0$ the model reproduces the linear-stability predicted $C_{Q_{min}}$ of $1.4 \cdot 10^{-5}$.

In computing $C_{Q_{min}}$, we have demanded that transition be delayed indefinitely, i.e., that

$$Re_{x_t} \to \infty \tag{39}$$

It is instructive to compute a family of $C_{Q_{min}}$ curves for the less stringent condition

$$Re_{x_t} > R_{min} \tag{40}$$

where R_{min} is a specified minimum Reynolds number below which transition is to be prevented. Such a family of curves was constructed; results are shown in Figure 9. Consistent with the Lang[18] data, provided T' is not too large, $C_{Q_{min}}$ of the order of .0001-.0003 is sufficient to stabilize a FPBL up to Reynolds numbers of a few million. However, for a fixed turbulence level, achieving values of Re_{x_t} beyond 10 million requires more suction. To see this quantitatively, $C_{Q_{min}}$ is replotted in Figure 10 with T' held constant on each curve. As an example, when T' = 0.10%, a value of $C_{Q_{min}} = .0001$ is sufficient to delay transition to $Re_{x_t} \sim 6 \cdot 10^6$ while $C_{Q_{min}}$ must increase by a factor of almost five in order to have $Re_{x_t} = 200 \cdot 10^6$.

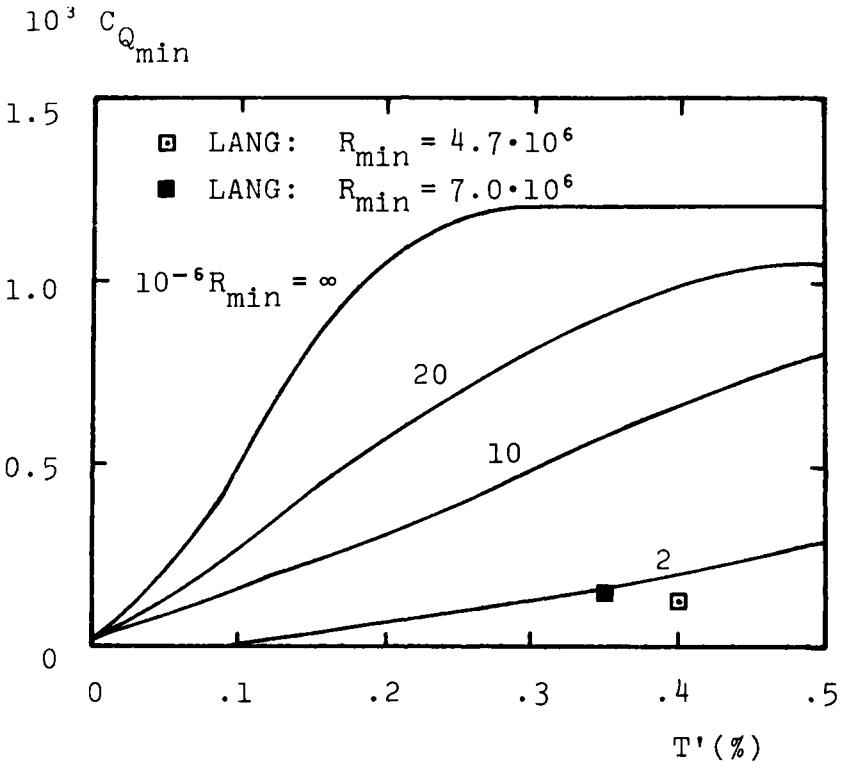

Figure 9. Predicted variation with freestream turbulence intensity of the minimum volume coefficient required to delay transition on a flat-plate boundary layer with uniform suction.

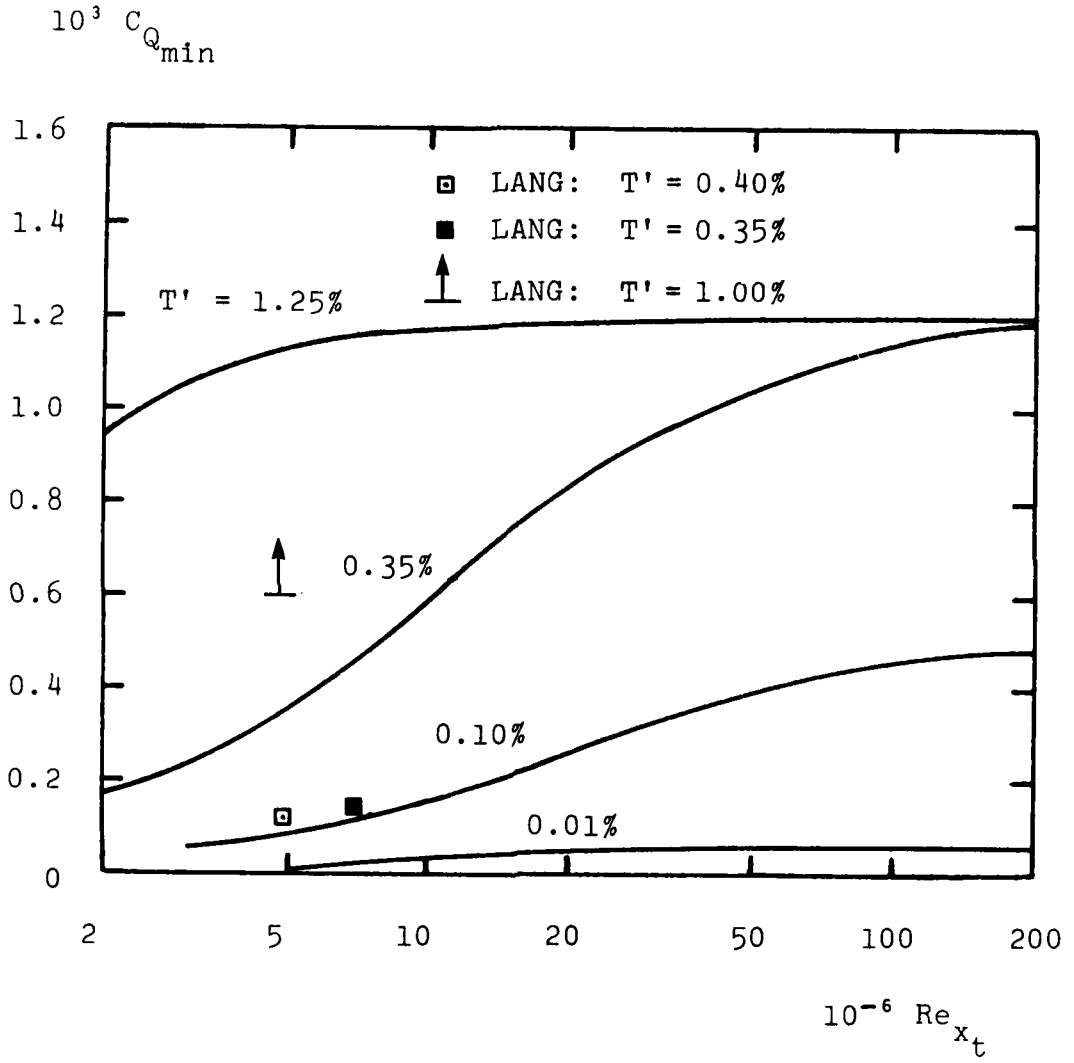

Figure 10. $C_{Q_{min}}$ as a function of Re_{x_t} for various freestream intensities, T'.

3.5 SURFACE HEAT TRANSFER

As our final boundary-layer application we now turn to effects of surface heat transfer on aerodynamic boundary-layer transition. Figure 11 compares computed and measured transition Reynolds number for low-speed aerodynamic boundary layers. The data of Zysina-Molozhen and Kuznetsova[19] were taken in relatively noisy environments so that they correspond to high intensity freestream conditions. The fact that the curve computed with $T' = 1.25\%$ is close to the data is hence very encouraging. For low intensity computations ($T' = 0.03\%$), the predicted stabilizing effect of cooling is much stronger than for the $T' = 1.25\%$ computations. As expected, the variation of $\left(Re_{x_t}\right)_w$ is approaching the linear stability predictions of Mack.[8]

Because ν_w increases with T_w, a subtle feature of surface heating effects on transition is masked by displaying $\left(Re_{x_t}\right)_w = U_e x_t/\nu_w$ as a function of T_w/T_e. Specifically, as the heating rate decreases, x_t initially increases, achieves a maximum, and eventually decreases. Figure 12 shows $\left(Re_{x_t}\right)_e = U_e x_t/\nu_e$ as a function of T_w/T_e for the $T' = 1.25\%$ calculation. As shown, for $T_w/T_e < 0.5$, additional cooling destabilizes the boundary layer. This trend is consistent with linear stability predictions.

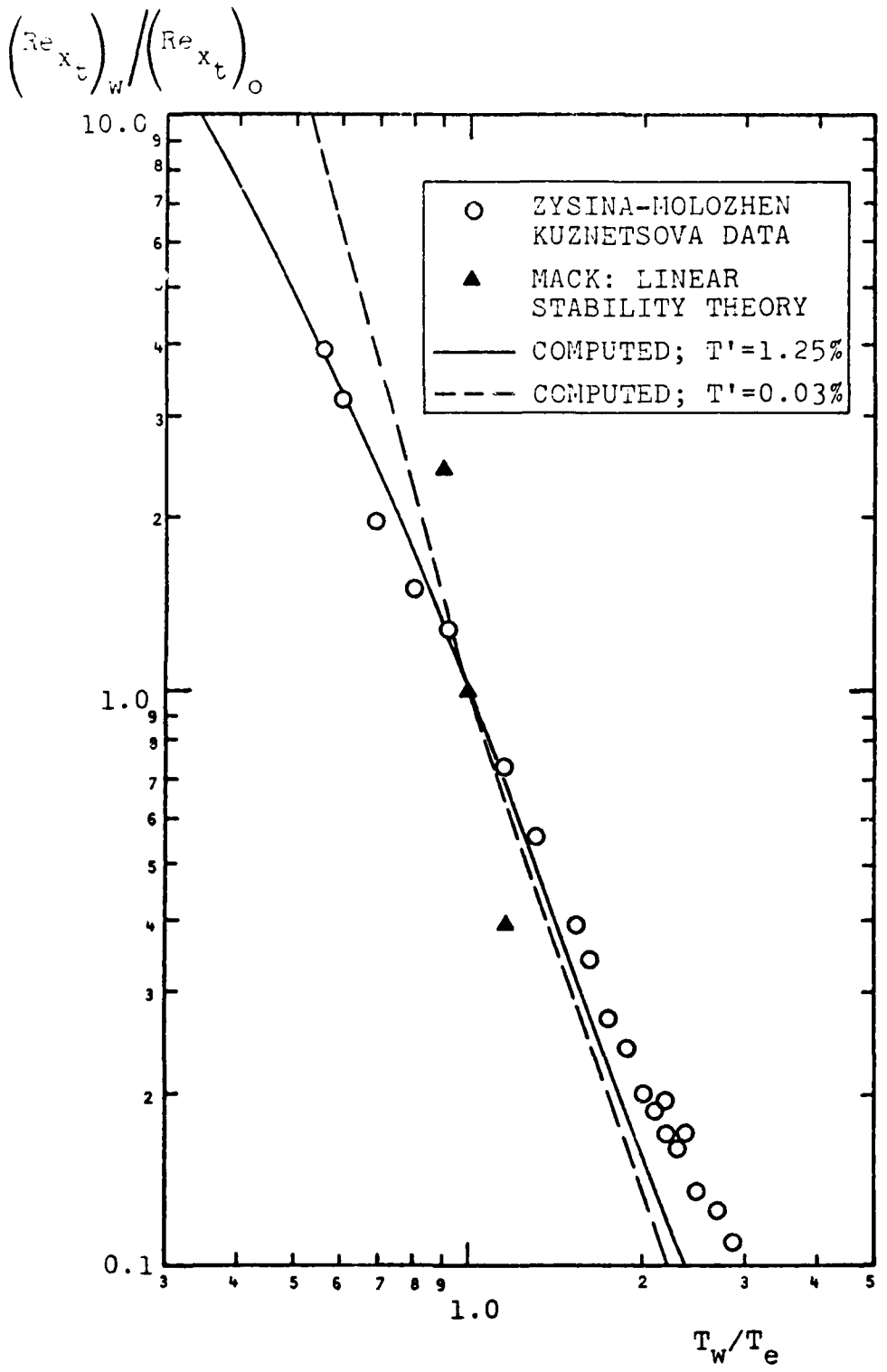

Figure 11. Comparison of computed and measured effects on transition of heat-transfer on low-speed aerodynamic boundary layers.

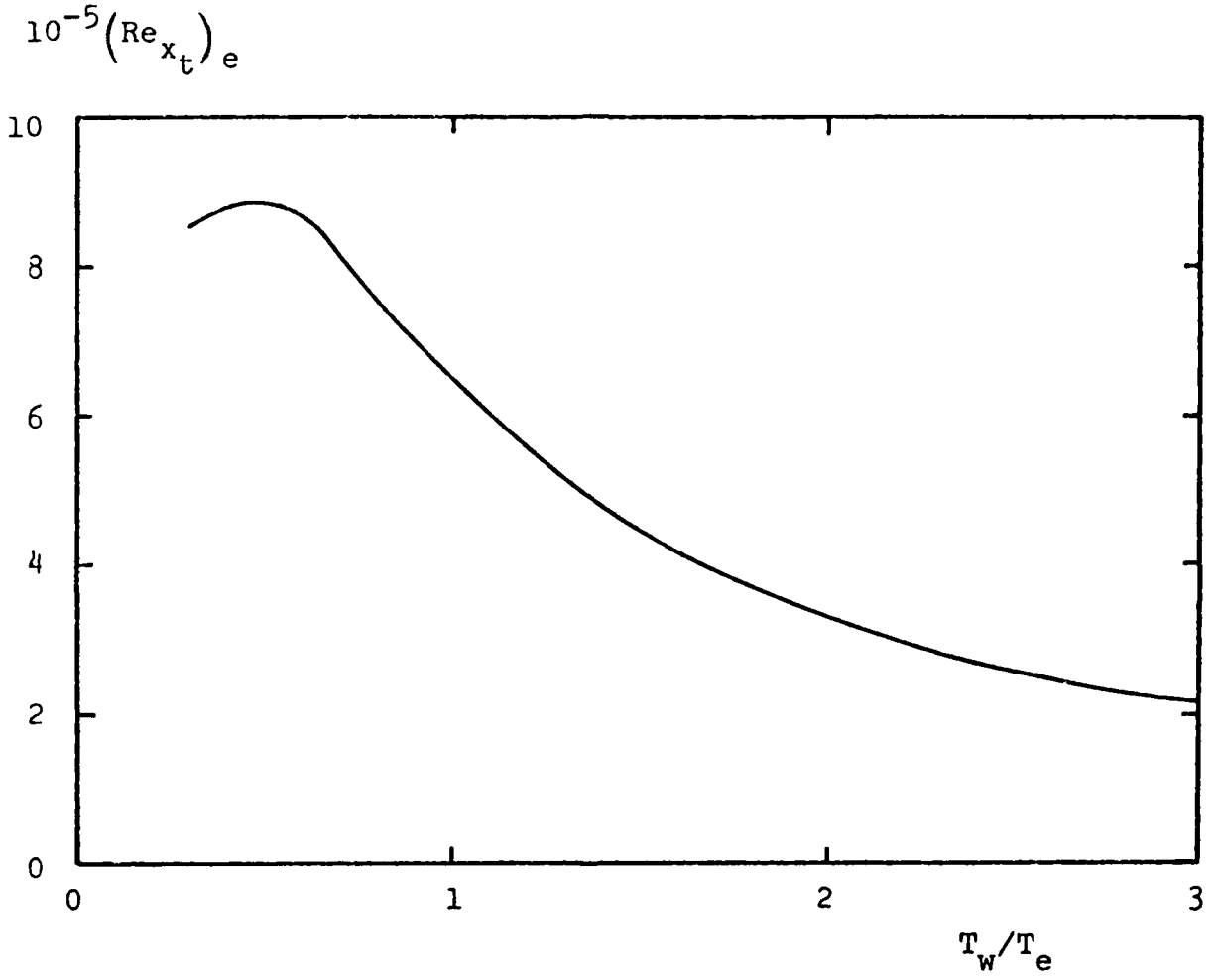

Figure 12. Predicted transition Reynolds number as a function of surface heat transfer for a low-speed aerodynamic boundary layer; T' = 1.25%.

4. HYDRODYNAMIC BODY APPLICATIONS

Having tested the model for well-documented incompressible flows on simple flat-plate geometries, we now turn to practical hydrodynamic designs. Computations presented in this section have been performed with virtually no advance knowledge of either linear-stability predictions or experimental data. The section consists of two parts. First, we simulate transition on four unheated hydrodynamic bodies; transition location is presented for each body over a range of freestream velocities. Then, for two of the bodies, the stabilizing effect of surface heating on transition is predicted.

4.1 UNHEATED BODIES

Four typical, axisymmetric low-drag bodies have been considered. Figure 13 depicts the body shapes and Douglas-Neumann computed pressure distributions. In the figure, L denotes body length measured along the symmetry axis, s_{mr} is the arclength at which the body radius is a maximum, and r_m is the maximum body radius. Also, C_p is the pressure coefficient defined by

$$C_p = \frac{p-p_\infty}{\frac{1}{2}\rho U_\infty^2} \tag{41}$$

Computations have been performed with molecular viscosity and laminar Prandtl number given by values appropriate for water near room temperature,[3] viz,

$$\mu = 7.943 \cdot 10^{-6}(T/600)^{-8} \text{ lb}\cdot\text{sec/ft}^2 \tag{42}$$

$$Pr_L = 2.51(T/600)^{-8} \tag{43}$$

with T in degrees Rankine. Freestream turbulence intensity is assumed to be

$$T' = .025\% \tag{44}$$

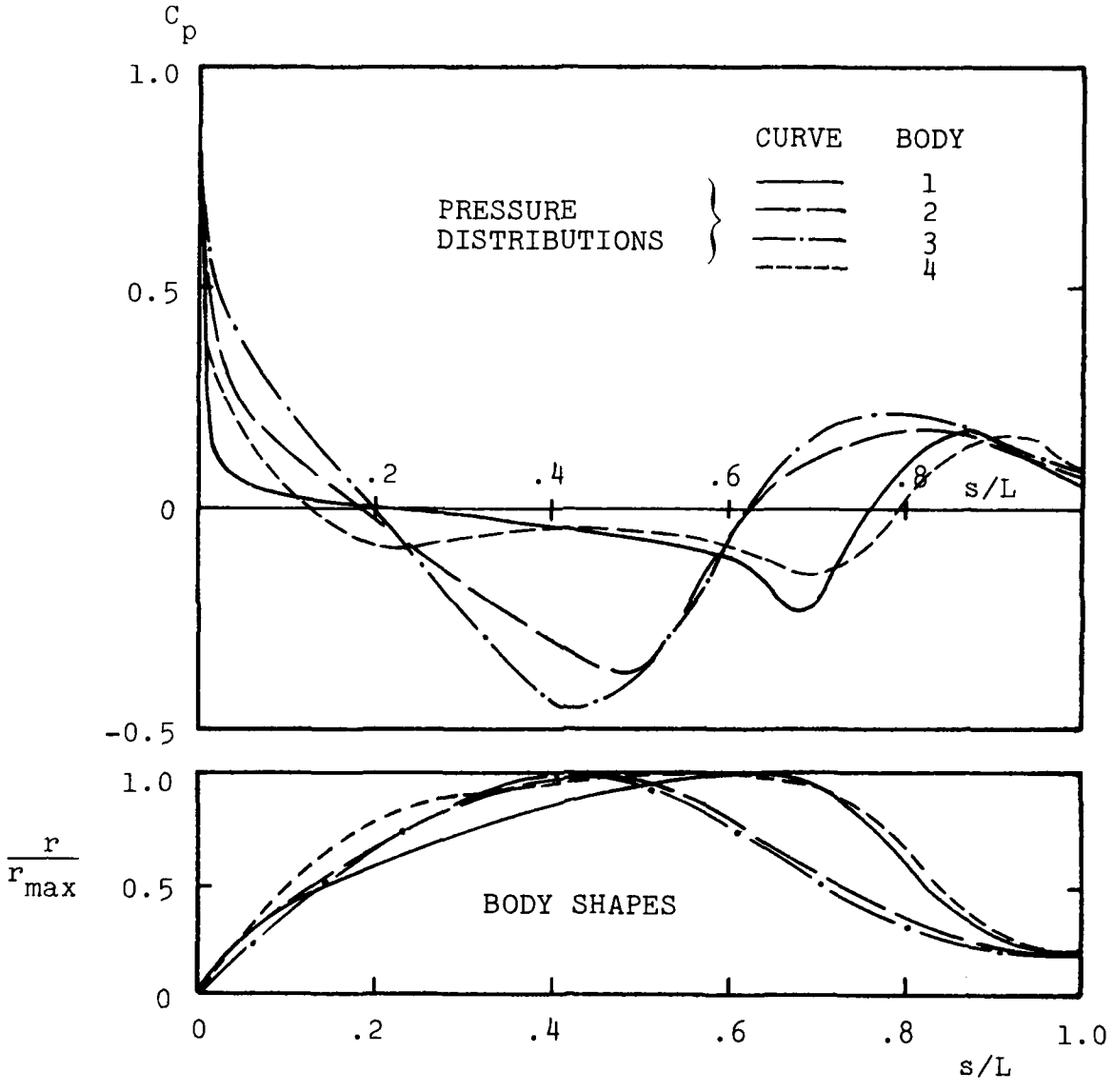

Figure 13. Body shapes and pressure distributions for the four low-drag hydrodynamic bodies.

and ℓ_e is given by Equation (36). Some of the computations have been repeated with T' = .01% and $\ell_e/\sqrt{\alpha^*_\infty}\,\delta = .09$; transition Reynolds numbers changed by less than 12%. Roughness heights of zero, 16 μin and 48 μin have been used; variation of k over this range produces a negligible effect on transition.

Inspection of Figure 13 shows that Bodies 1, 2 and 3 have progressively strong favorable pressure gradients ahead of the maximum radius (minimum pressure). Body 4 has a mild favorable gradient up to $s/s_{mr} \doteq 0.41$, followed by a slight adverse gradient from $s/s_{mr} \doteq 0.41$ to $s/s_m \doteq 0.73$, and subsequently a favorable pressure gradient up to the pressure minimum. Intuitively, we expect to find increasing transition Reynolds number as we proceed from Body 1 to Body 3. For Body 4, we expect transition will occur either upstream of or very near the beginning of the adverse pressure gradient on the forebody.

Model predictions for the four bodies confirm our intuitive notions. Figure 14 presents transition arclength, s_t, as a function of volume Reynolds number, $Re_{V^{1/3}}$, defined by

$$Re_{V^{1/3}} \equiv \rho U_\infty V^{1/3}/\mu_\infty \qquad (45)$$

For Body 1, transition occurs ahead of laminar separation for $Re_{V^{1/3}}$ in excess of about 2 million. Because of Body 2's stronger favorable pressure gradient, transition does not move ahead of laminar separation until $Re_{V^{1/3}}$ exceeds 9.8 million. For the even stronger favorable gradient of Body 3, although transition appears just upstream of laminar separation at $Re_{V^{1/3}} = 6.5$ million, transition occurs downstream of minimum pressure at the highest Reynolds number considered, namely 15 million. Finally, for Body 4, the adverse pressure gradient on the forebody triggers transition at the lowest Reynolds numbers considered; for the higher Reynolds numbers transition occurs upstream of the adverse gradient. Table 1 summarizes results of the computations.

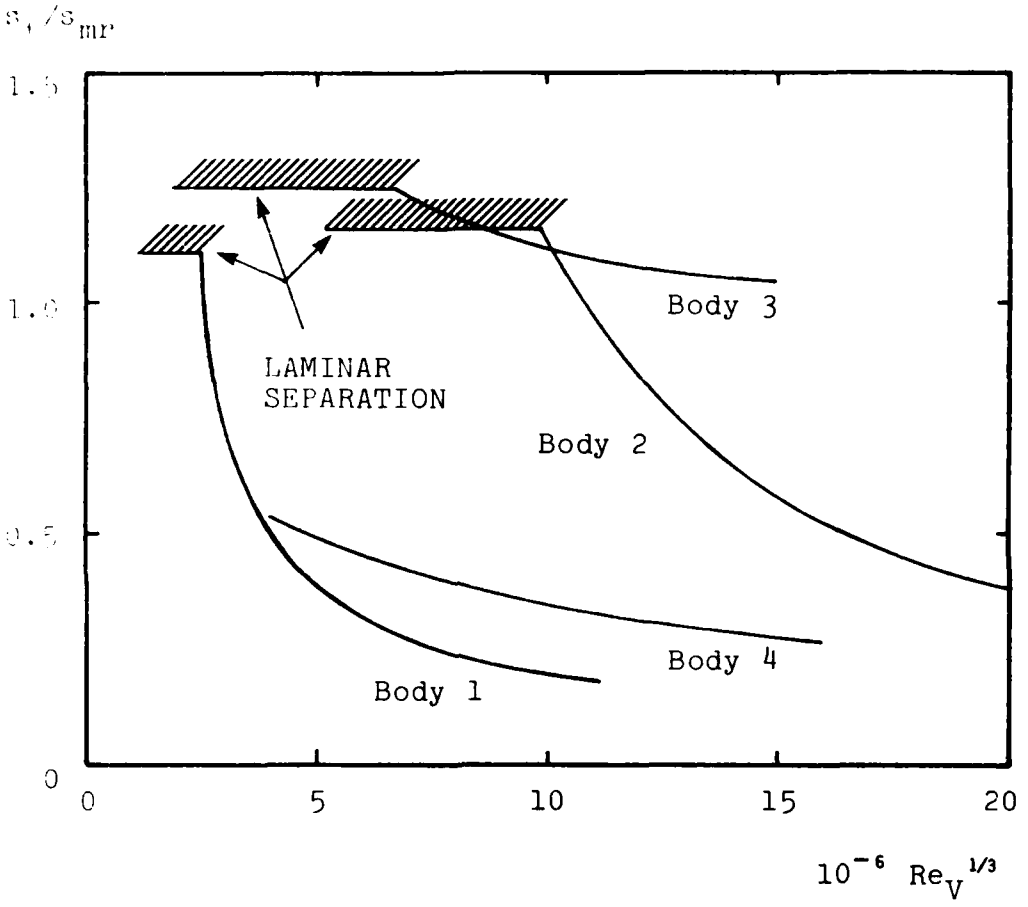

Figure 14. Transition location for the four hydrodynamic bodies without surface heating.

Table 1. Summary of transition predictions for the unheated bodies.

Body Number	10^{-6} $Re_{V^{1/3}}$	s_t/s_{mr}	10^{-6} Re_{s_t}
1	1.12	1.108*	4.68*
↓	2.79	0.841	8.43
	5.57	0.346	6.67
	11.17	0.178	6.78
2	5.19	1.160*	12.23*
↓	10.36	1.070	22.98
	11.97	0.847	20.28
	13.97	0.661	17.63
	15.17	0.568	16.05
	17.17	0.471	14.63
	19.95	0.378	13.22
3	1.88	1.253*	4.14*
↓	5.63	1.253*	12.50*
	9.34	1.140	19.13
	13.14	1.059	25.39
	15.02	1.049	28.75
4	3.98	0.535	6.55
↓	7.96	0.389	9.61
	11.93	0.315	11.60
	15.91	0.264	12.77

*Laminar separation.

4.2 HEATED BODIES

For Bodies 2 and 4, computations have been repeated with various amounts of surface heating. Two heating distributions have been considered for Body 2. For both distributions there is no heating up to $s = s_{min}$, uniform heating from $s = s_{min}$ to $s = s_{max}$, and no heating beyond $s = s_{max}$ (see insert in Figure 15); $s_{min}/s_{mr} = .46$ for the first distribution while $s_{min}/s_{mr} = .17$ for the second distribution. The heating distributions for Body 4 are those predicted by linear-stability theory as being the minimum heating required to prevent transition from occurring ahead of laminar separation.

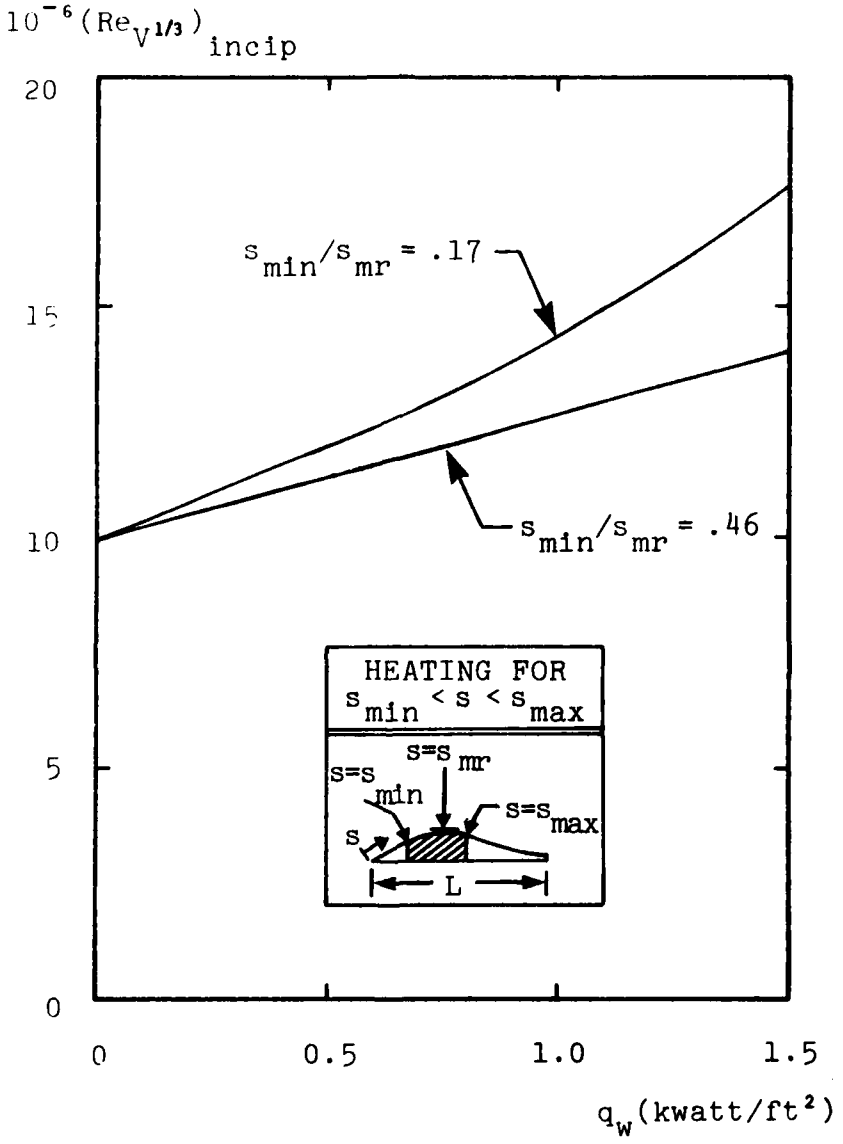

Figure 15. Effect of surface heating on incipient transition Reynolds number for Body 2.

Figure 15 and Table 2 present results of the computations for Body 2. Incipient transition Reynolds number, $(Re_{V^{1/3}})_{incip}$, (i.e., the value at which transition and laminar separation points coincide) has been predicted as a function of heating rate. As shown, when $s_{min}/s_{mr}=.46$ a modest increase in $(Re_{V^{1/3}})_{incip}$ is observed. Moving s_{min} closer to the nose causes a more dramatic increase in $(Re_{V^{1/3}})_{incip}$. This trend is in qualitative agreement with measurements.

Table 2. Summary of transition predictions for Body 2 with surface heating.

s_{min}/s_{mr}	q_w(kwatt/ft^2)	$10^{-6}(Re_{V^{1/3}})_{incip}$	$10^{-6}\,Re_{s_t}$
.46 ↓	0	9.8	22.0
	.75	12.0	28.0
	1.50	14.0	33.0
.17 ↓	0	9.8	22.0
	.75	13.0	32.0
	1.50	17.6	40.3

Figure 16 and Table 3 summarize results for Body 4 with surface heating. At the two lowest Reynolds numbers, transition has been prevented upstream of laminar separation. For $Re_{V^{1/3}} = 11.93$, transition is predicted between the minimum pressure and laminar separation points while, at the highest Reynolds number considered, transition occurs just upstream of minimum pressure. Again, predictions are in qualitative agreement with measurements.

Table 3. Summary of transition predictions for body 4 with surface heating.

$10^{-6}\,Re_{V^{1/3}}$	s_t/s_{mr}	$10^{-6}\,Re_{s_t}$
3.98	1.276*	15.91*
7.96	1.276*	32.10*
11.93	1.196	45.54
15.91	0.951	46.51

*Laminar separation.

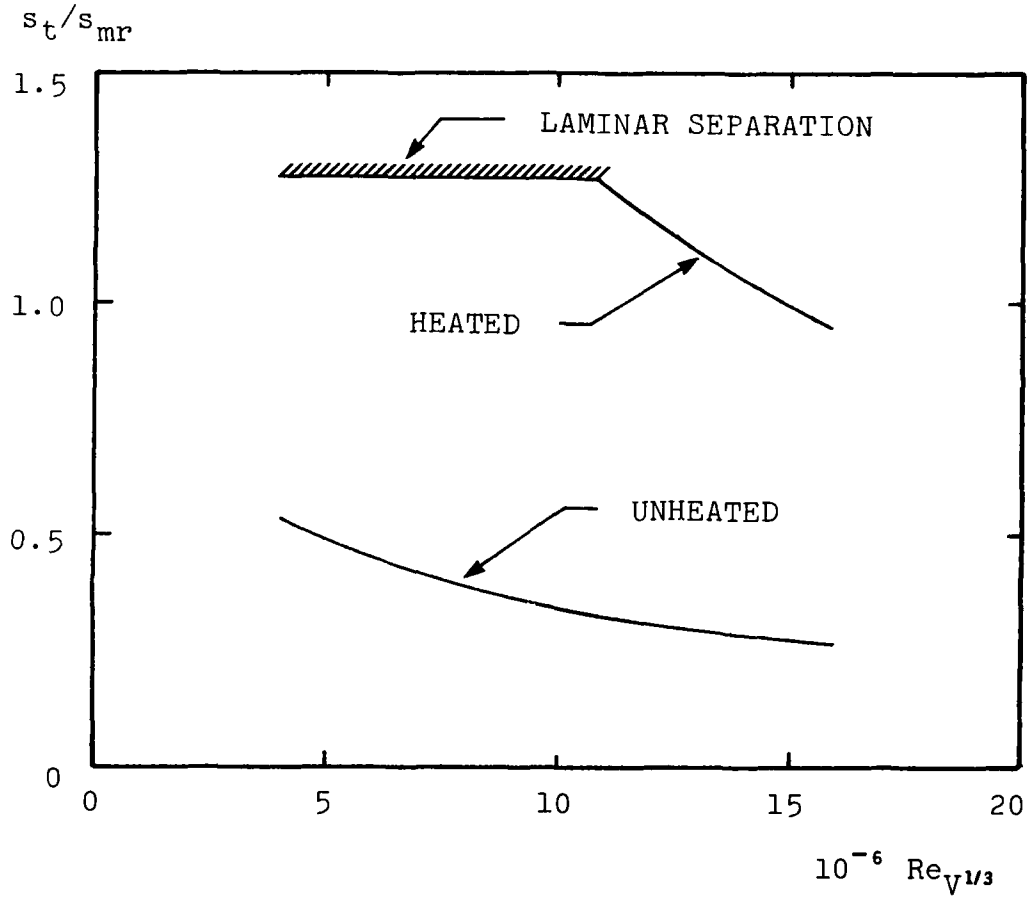

Figure 16. Transition location for Body 4 with and without surface heating.

5. DISCUSSION

Results presented in Sections 3 and 4 lend further confidence to the turbulence-model transition-prediction method. The model accurately simulates transition sensitivity to many of the effects pertinent to low-drag hydrodynamic bodies. While detailed comparisons between predicted and measured transition points for the hydrodynamic bodies analyzed in Section 4 have not been presented, early indications are that an acceptable level of accuracy has been obtained.

The explanation for the manner in which Tollmien-Schlichting waves manifest themselves in the theory (Subsection 2.4) puts the model in much clearer perspective than previously realized. Most notably, by using linear stability theory to determine the closure coefficient λ for a given flow the model could be the basis of a plausible alternative to the e^9 procedure. Predictions remain relatively sensitive to freestream turbulence intensity, a sensitivity which probably will remain uncertain until more extensive experimental data become available.

In conclusion, success achieved in this study coupled with prior success in predicting trnasition on Mach 5 ground-test[5] and Mach 20 flight-test vehicles[6] further substantiates the notion that the method can be used as a design tool for a wide range of aerodynamic/hydrodynamic vehicles.

APPENDIX: NEAR-SURFACE BEHAVIOR OF SOLUTIONS TO THE MODEL EQUATIONS

This Appendix presents an analytical solution to the turbulence model equations which is valid very near a solid boundary. To determine how far from a solid boundary the analytical solution applies, numerical solutions to the model equations have been generated for a variety of laminar, transitional and turbulent boundary layers. As a result, the required number of mesh points needed for accurate numerical solution has been reduced with an attendant reduction in computing time.

Computations with DCW Industries' EDDYBL computer code, which embodies the turbulence model equations, generally require mesh points extremely close to a solid boundary to insure accurate computation of the turbulent dissipation rate, ω. The reason for having very fine resolution near the boundary is the singular behavior of ω at very smooth surfaces. For incompressible flow over a rough surface, Saffman and Wilcox[20] have shown that

$$\omega \doteq \omega_w \left[1 + \sqrt{40S}\,\frac{u_\tau y}{\nu}\right]^{-2} \tag{A1}$$

where ω_w is the value at the surface. The quantity S is the universal function of surface roughness and mass injection defined in Equations (19)-(21); for $v_w = 0$ and for small roughness heights, k, S is

$$S \doteq \left(\frac{36}{u_\tau k/\nu}\right)^2 \tag{A2}$$

Note that for a perfectly smooth surface

$$\omega \to y^{-2} \quad \text{as} \quad y \to 0 \tag{A3}$$

It is therefore a y^{-2} singularity we are forced to resolve in EDDYBL computations.

If the analytical behavior of ω is accurately represented by Equations A1 and A2, we could obviate the stringent resolution problem by using these equations rather than computing ω with finite differences. Hence, efforts focused first upon generalizing Equation A1 for flows with heat transfer and then testing the accuracy of the formula for several flows.

Using singular perturbation techniques we find that the generalized solution for flows with heat transfer is

$$\omega = \omega_w \left[1 + \sqrt{40S}\, \frac{u}{u_\tau} \right]^{-2} \qquad (A4)$$

where u is velocity. Note that for incompressible flat-plate boundary layers

$$u/u_\tau = u_\tau y/\nu \quad \text{as} \quad u_\tau y/\nu \to 0 \qquad (A5)$$

wherefore Equation A4 reduces to Equation A1.

To test the accuracy of Equation A4, boundary layer computations have been performed for a variety of flows including incompressible and compressible FPBL's, incompressible FPBL with uniform blowing, and flow over Body 2 with heating. As shown in Figures A1 and A2, with the exception of the blowing case, Equation A4 is accurate for values of u/u_τ below about 4. For the blowing case, Equation A4 is valid to about $u/u_\tau = 1$.

Hence, Equation A4 can be used for computing ω below u/u_τ of about 4 for the flows of interest in this study (incompressible, smooth wall). Rather than having to place mesh points as close to the wall as $u_\tau y/\nu = 1/10$, there is no need to have points any closer than $u_\tau y/\nu = 1$. This results in a substantial (factor of 2) decrease in computing time.

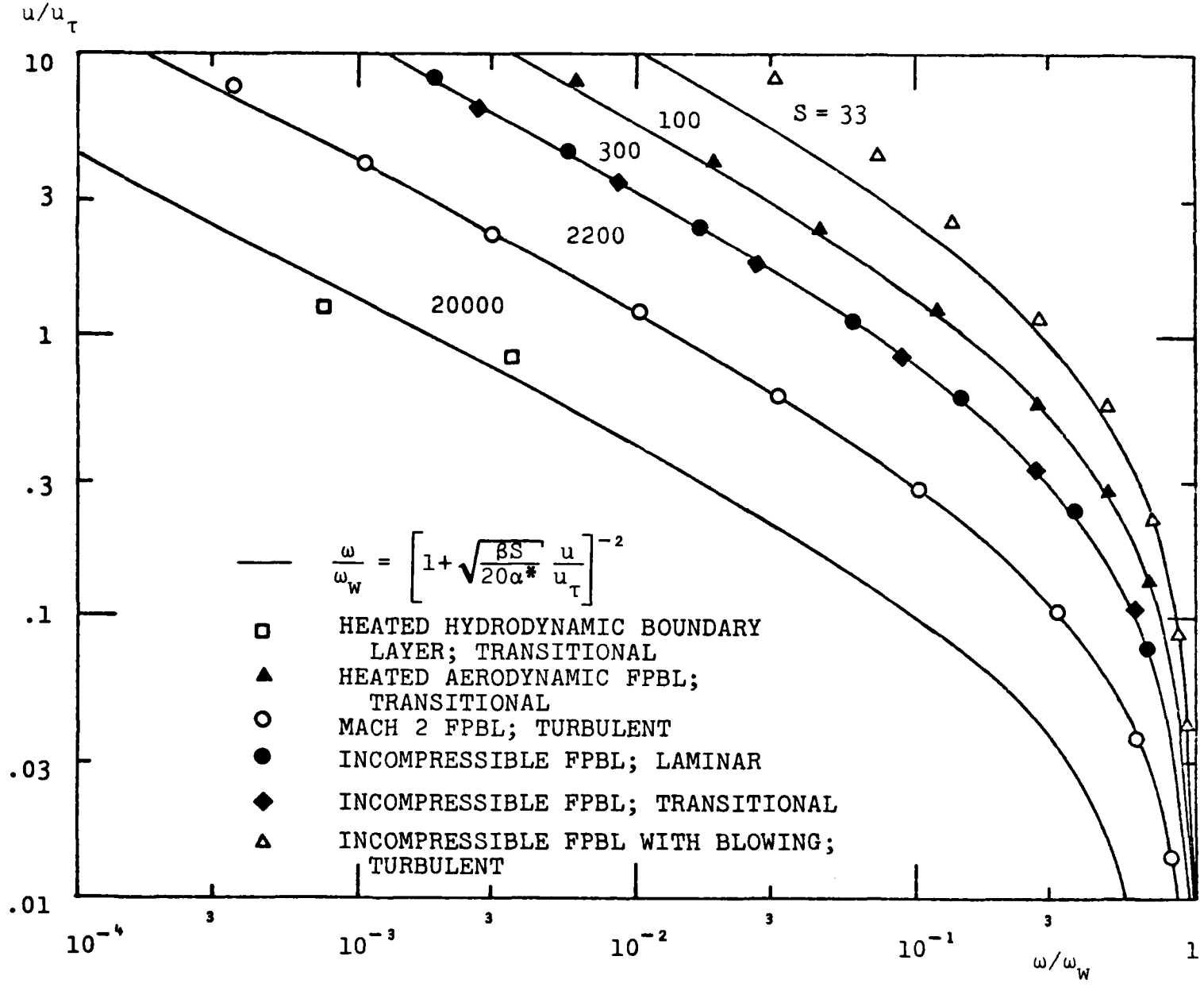

Figure A1. Comparison of computed near-surface dissipation-rate variation with the theoretical solution.

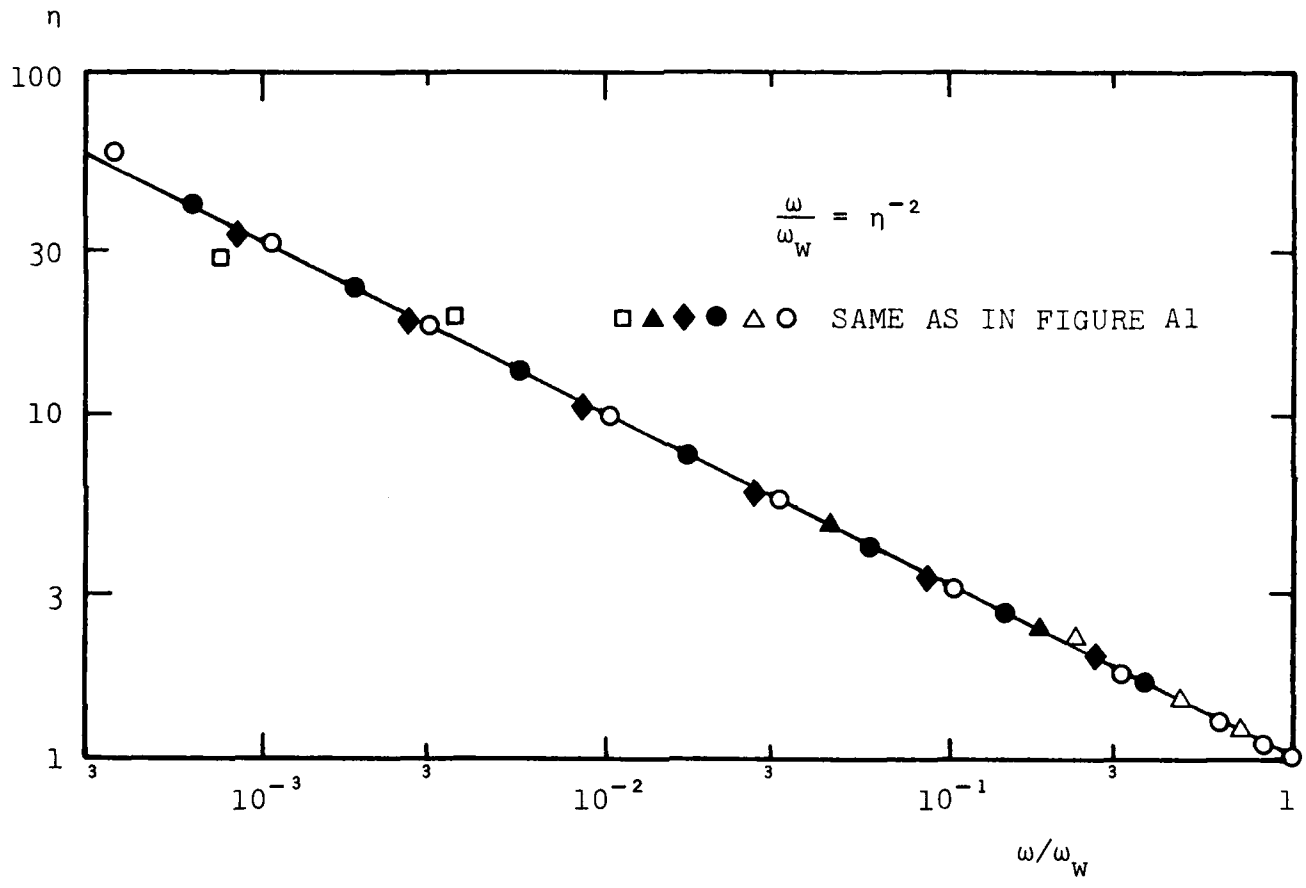

Figure A2. Comparison of computed near-surface dissipation-rate variation with that predicted by the theoretical solution.

REFERENCES

1. Wilcox, D.C., "Turbulence Model Transition Predictions," AIAA Journal, Vol 13, No 2, pp 241-243 (Feb 1975).

2. Wilcox, D.C., "Turbulence Model Transition Predictions: Effects of Surface Roughness and Pressure Gradient," AIAA Paper 75-857 (June 1975).

3. Wilcox, D.C. and Chambers, T.L., "Effects of Surface Heat Transfer on Boundary-Layer Transition," AFOSR-TR-75-1398 (July 1975).

4. Wilcox, D.C. and Chambers, T.L., "Further Refinement of the Turbulence-Model Transition-Prediction Technique," AFOSR-TR-75-1682 (July 1975).

5. Wilcox, D.C. and Chambers, T.L., "Numerical Simulation of Nosetip Transition: Model Refinement and Validation," DCW Industries Report DCW-R-03-04 (July 1976).

6. Chambers, T.L. and Wilcox, D.C., "Application of the Turbulence-Model Transition-Prediction Method to Flight-Test Vehicles," DCW Industries Report DCW-R-12-01 (June 1976).

7. Schlichting, H., Boundary Layer Theory, Fourth Ed, McGraw-Hill, New York, p 414 (1960).

8. Personal communication between L.M. Mack of JPL and D.C. Wilcox of DCW Industries (Feb 1976).

9. Smith, A.M.O. and Gamberoni, N., "Transition, Pressure Gradient, and Stability Theory," Report ES 26388, Douglas Aircraft Co, Inc, El Segundo, CA (1956).

10. Morkovin, M.V., "Critical Evaluation of Transition from Laminar to Turbulent Shear Layers with Emphasis on Hypersonically Traveling Bodies," AFFDL-TR-68-149 (Mar 1969).

11. Dryden, H.L., Aerodynamics and Jet Propulsion, Vol V, University Press, Princeton, NJ (1959).

12. Dhawan, S. and Narasimha, R., "Some Properties of Boundary Layer Flow During the Transition from Laminar to Turbulent Motion," Journal of Fluid Mechanics, Vol 3, Pt 4, pp 418-436 (1958).

13. Schubauer, G.B. and Klebanoff, P.S., "Contributions on the Mechanics of Boundary Layer Transition," NACA 1289 (1956).

14. Feindt, E.G., "Untersuchungen über die Abhängigkeit des Umschlages Laminar-Turbulent von der Oberflächenrauhigkeit und der Druckverteilung," Thesis Braunschweig 1956; Jahrbuch 1956 der Schiffbautech nischen Gesellschaft 50, pp 180-203 (1957)

15. Crabtree, L.F., "Prediction of Transition in the Boundary Layer on an Aerofoil," Journal Roy Aero Soc, Vol 62, p 525 (1958).

16. Simpson, R.L., Moffatt, R.J. and Kays, W.M., "The Turbulent Boundary Layer on a Porous Plate: An Experimental Study of the Fluid Dynamics with Suction and Injection," Univ Stanford Thermosciences Div Rept HMT-2, Stanford Univ (1972).

17. Pfenninger, W. and Bacon, J.W., "Investigation of Methods for Re-Establishment of a Laminar Boundary Layer from Turbulent Flow," Northrop Report NOR 65-48, Northrop Corp, Hawthorne, CA (1965).

18. Personal communication between T.G. Lang of Naval Underseas Center, San Diego, CA, and D.C. Wilcox of DCW Industries (Sept 1976).

19. Zysina-Molozhen, L.M. and Kuznetsova, V.M., "Investigation of Turbulent Conditions in a Boundary Layer," Thermal Engineering (Teploenergetika), Vol 16, No 7, pp 16-20 (1969).

20. Saffman, P.G. and Wilcox, D.C., "Turbulence-Model Predictions for Turbulent Boundary Layers," AIAA Journal, Vol 12, No 4, pp 541-546 (1974).

UNCLASSIFIED

SECURITY CLASSIFICATION OF THIS PAGE *(When Data Entered)*

REPORT DOCUMENTATION PAGE		READ INSTRUCTIONS BEFORE COMPLETING FORM
1. REPORT NUMBER	2. GOVT ACCESSION NO. AD-A134 941	3. RECIPIENT'S CATALOG NUMBER
4. TITLE *(and Subtitle)* TRANSITION SIMULATION FOR INCOMPRESSIBLE BOUNDARY LAYERS AND HEATED HYDRODYNAMIC BODIES		5. TYPE OF REPORT & PERIOD COVERED Final Scientific Report
		6. PERFORMING ORG. REPORT NUMBER DCW-R-10-01
7. AUTHOR(s) D.C. Wilcox and T.L. Chambers		8. CONTRACT OR GRANT NUMBER(s) Contract N00024-76-C-7070
9. PERFORMING ORGANIZATION NAME AND ADDRESS DCW Industries 13535 Ventura Boulevard, Suite 207 Sherman Oaks, CA 91423		10. PROGRAM ELEMENT, PROJECT, TASK AREA & WORK UNIT NUMBERS
11. CONTROLLING OFFICE NAME AND ADDRESS Department of the Navy Naval Sea Systems Command Washington, D.C. 20362		12. REPORT DATE July 1976
		13. NUMBER OF PAGES 54
14. MONITORING AGENCY NAME & ADDRESS*(if different from Controlling Office)* Defense Advanced Research Projects Agency Arlington, Virginia 22209		15. SECURITY CLASS. *(of this report)* Unclassified
		15a. DECLASSIFICATION/DOWNGRADING SCHEDULE
16. DISTRIBUTION STATEMENT *(of this Report)*		
17. DISTRIBUTION STATEMENT *(of the abstract entered in Block 20, if different from Report)*		
18. SUPPLEMENTARY NOTES		
19. KEY WORDS *(Continue on reverse side if necessary and identify by block number)*		

20. ABSTRACT *(Continue on reverse side if necessary and identify by block number)*

Incompressible boundary-layer transition has been analyzed using a second-order closure turbulence model. With no transition-specific modifications, the turbulence model predicts salient features of incompressible, zero-pressure-gradient boundary-layer transition including sensitivity to freestream turbulence and surface roughness, transition width, and transitional velocity profiles. With transition modifications based on linear stability

DD FORM 1 JAN 73 1473 EDITION OF 1 NOV 65 IS OBSOLETE

UNCLASSIFIED

SECURITY CLASSIFICATION OF THIS PAGE *(When Data Entered)*

theory, the model accurately predicts transition sensitivity to surface heat transfer, pressure gradient, and suction. With no further modifications, transition predictions have been made for several hydrodynamic bodies, including effects of surface heating.

END

FILMED

12-83

DTIC